объединенный
институт
ядерных
исследований
дубна

E15-94-343

Ableev V.G.

MEASUREMENTS OF THE $\bar{p}d$ ANNIHILATION AT REST

OBELIX Collaboration

Submitted to «Nuclear Physics A»

1994

V.G.Ableev[1], M.Agnello[3], F.Balestra[4], G.Bendiscioli[5], A.Bertin[6], P.Boccaccio[7], E.Botta[4], T.Bressani[4], M.Bruschi[6], M.P.Bussa[4], L.Busso[4], D.Calvo[4], M.Capponi[6], B.Cereda[6], P.Cerello[4], C.Cicalo[2], S.Costa[4], S.De Castro[6], O.Yu.Denisov[1], D.D'Isep[4], A.Donzella[9], L.Fava[4], A.Feliciello[4], L.Ferrero[4], A.Filippi[4], V.Filippini[5], A.Fontana[5], D.Galli[6], R.Garfagnini[4], U.Gastaldi[7], B.Giacobbe[6], P.Gianotti[8], O.E.Gorchakov[1], A.Grasso[4], C.Guaraldo[8], F.Iazzi[3], A.Lanaro[8], E.Lodi Rizzini[9], M.Lombardi[7], V.Lucherini[8], A.Maggiora[4], G.Maneva[1], S.Marcello[4], U.Marconi[6], G.V.Margagliotti[10], G.Maron[7], A.Masoni[2], B.Minetti[3], P.Montagna[5], M.Morando[11], F.Nichitiu[1,8], D.Panzieri[4], G.Pauli[10], M.Piccinini[6], M.Poli[12], S.N.Prakhov[1], G.Puddu[2], R.A.Ricci[7,11], E.Rossetto[14], A.Rotondi[5], A.M.Rozhdestvensky[1], A.Saino[5], P.Salvini[5], L.Santi[13], M.G.Sapozhnikov[1], N.Semprini-Cesari[5], S.Serci[2], R.Spighi[6], P.P.Temnikov[2], S.Tessaro[10], F.Tosello[4], V.I.Tretyak[1,5], G.Usai[2], L.Vannucci[7], S.Vecchi[6], G.Vedovato[7], L.Venturelli[9], M.Villa[6], A.Vitale[6], A.Zenoni[14], A.Zoccoli[6], G.Zosi[4]

[1]Joint Institute for Nuclear Research, Dubna, Russia
[2]Dipartimento di Scienze Fisiche, Universita di Cagliari and INFN, Sezione di Cagliari, Cagliari, Italy
[3]Politecnico di Torino and INFN, Sezione di Torino, Italy
[4]Dipartimento di Fisica, Universita di Torino and INFN, Sezione di Torino, Torino, Italy
[5]Dipartimento di Fisica Nucleare e Teorica, Universita di Pavia and INFN, Sezione di Pavia, Pavia, Italy
[6]Dipartimento di Fisica, Universita di Bologna and INFN, Sezione di Bologna, Bologna, Italy
[7]Laboratori Nazionali di Legnaro dell'INFN, Legnaro, Italy
[8]Laboratori Nazionali di Frascati dell'INFN, Frascati, Italy
[9]Dipartimento di Elettronica per l'Automazione, Universita di Brescia and INFN, Sezione di Torino, Italy
[10]Istituto di Fisica, Universita di Trieste and INFN, Sezione di Trieste, Trieste, Italy
[11]Dipartimento di Fisica, Universita di Padova and INFN, Sezione di Padova, Padova, Italy
[12]Dipartimento di Energetica, Universita di Firenze and INFN, Sezione di Bologna, Bologna, Italy
[13]Istituto di Fisica, Universita di Udine and INFN, Sezione di Trieste, Italy
[14]Dipartimento di Elettronica per l'Automazione, Universita di Brescia and INFN, Sezione di Pavia, Italy

1 Introduction

We report the measurements of annihilation of stopped antiprotons in a deuterium gas target performed with the OBELIX spectrometer at LEAR (CERN). The main physical motivation for these measurements was to study ϕ-meson production in $\bar{N}N$ annihilation. It has been stimulated by the experimental data [1]-[3] showing that the yield of ϕ in $\bar{p}p$ annihilation is remarkably high and the ratio between ϕ-meson and ω-meson production is larger than expectation from the OZI-rule [4]. Moreover, these data demonstrate the highest degree of the OZI-rule violation among all other hadron interactions at different energies.

Indeed, according to the OZI-rule, it was predicted [5] that

$$R = \frac{B.R.(\bar{N}N \to \phi X)}{B.R.(\bar{N}N \to \omega X)} = \tan^2\delta \tag{1}$$

where $\delta = \theta - \theta_i$ is the deviation from the ideal mixing angle $\theta_i = 35.3^0$.

Since the vector mesons are practically ideally mixed, δ is small. Indeed the mixing angle from the quadratic Gell-Mann-Okubo mass formula is $\theta = 39^0$ and from the linear one it is $\theta = 36^0$ [6]. Substituting these values in (1) one obtains

$$\begin{aligned} R &= 4.2 \cdot 10^{-3} \quad \text{for the quadratic mass formula} \\ R &= 0.15 \cdot 10^{-3} \quad \text{for the linear mass formula} \end{aligned} \tag{2}$$

These predictions are in sharp contrast with the recent data on $\bar{p}p$ annihilation at rest. The ASTERIX collaboration [2] found that the ratio $\phi\pi/\omega\pi$ for annihilation from the S-wave was as high as $R = (76.9 \pm 17.1) \cdot 10^{-3}$. The Crystal Barrel collaboration [3] confirmed the violation of the OZI rule obtained by the ASTERIX group and found for the ratio $\phi\pi^0/\omega\pi^0$ the value $R = (140 \pm 40) \cdot 10^{-3}$. They also found especially high violation of the OZI rule for the $\phi\gamma/\omega\gamma$ ratio.

Indications on significant OZI-rule violation in antiproton annihilation on neutrons existed since the old bubble chamber experiments [7], [8], which had found a substantial yield of the $\phi\pi^-$ channel. Using the branching ratio for the $\bar{p}n \to \omega\pi^-$ channel from [9], [10], one could obtain $R = (83 \pm 25) \cdot 10^{-3}$. However the statistics in these experiments was rather scarce. For instance, in [7] only 54 events of the $\phi\pi^-$ channel were found.

Recently the OBELIX collaboration has measured the ϕ and ω meson production in the antineutron annihilations in liquid hydrogen [11]. A significant violation of the OZI-rule was found with $R = B.R.(\phi\pi^+)/B.R.(\omega\pi^+) = (110 \pm 15 \pm 6) \cdot 10^{-3}$.

We have investigated the following reactions

$$\bar{p} + d \longrightarrow \pi^- + \phi + p \tag{3}$$

$$\bar{p} + d \longrightarrow \pi^- + \omega + p \tag{4}$$

in the antiproton annihilation at rest on gaseous deuterium using the OBELIX spectrometer at LEAR (CERN).

The branching ratios of $\phi\pi^-$ and $\omega\pi^-$ channels were measured for two regions of proton momenta: $P < 200$ MeV/c and $P > 400$ MeV/c. Substantial violation of the OZI rule was found. The ratio R=$\phi\pi/\omega\pi$ is about 30 times higher than the theoretical prediction obtained following the quadratic mass formula.

As a by-product of the study of the ϕ-meson formation, which was performed with a dedicated trigger, we took data on antiproton deuterium annihilation at rest with a minimum bias trigger. It was possible to measure the branching ratios of the following reactions:

$$\bar{p} + d \longrightarrow 2\pi^- + \pi^+ + p \tag{5}$$

$$\bar{p} + d \longrightarrow 3\pi^- + 2\pi^+ + p \tag{6}$$

for two regions of proton momenta: $P < 200$ MeV/c and $P > 400$ MeV/c.

The possibility of exploring the high proton momentum region brought some interesting information concerning the dynamics of $\bar{p}d$-annihilation. For the first time the excitation of the Δ-resonance was observed among the final state products of $\bar{p}d$ annihilation.

A broad bump in 4π invariant mass at $m = 1497 \pm 8$ MeV with $FWHM = 177 \pm 14$ MeV was seen in reaction (6). A similar enhancement had been seen previously [12] and dubbed $\xi(1480)$. Later this bump was seen also by the ASTERIX collaboration [13], which found that the position of the peak changed with the increasing of the momentum of proton.

In our data we observed the same effect of the shifting of the bump position at ≈ 100 MeV down when the proton momentum increased up to $P > 400$ MeV/c. We also observed that the positions of ω, ρ and $f_2(1270)$ did not change with the proton momentum.

In the nucleon-spectator region ($P < 200$ MeV/c) the reactions

$$\bar{p} + d \longrightarrow 2\pi^- + 2\pi^+ + n \tag{7}$$

$$\bar{p} + d \longrightarrow 3\pi^- + 3\pi^+ + n \tag{8}$$

were studied and their branching ratios determined.

We also studied reactions with the Λ hyperon formation. The interest to study such processes comes from the fact that in the annihilation on a free nucleon, Λ production has a threshold at the antiproton momentum $P_{th} = 1436$ MeV/c. However, in the antiproton annihilation on nuclei, even antiprotons at rest could create Λ, via rescattering of the annihilation mesons (for a review, see [14]-[17]). So in our case both nucleons of the deuteron should participate in the process and it is interesting to establish the experimental features of such "two-body" annihilations.

In our data sample with proton momenta $P > 400$ MeV/c we have identified the following reactions of Λ production:

$$\bar{p} + d \longrightarrow \Lambda + K^+ + \pi^- \tag{9}$$

$$\bar{p} + d \longrightarrow \Lambda + K^+ + \pi^- + \pi^0 \tag{10}$$

and have studied their characteristics.

The paper is organized as follows. Section 2 contains the description of the OBELIX experimental apparatus. The procedure of the data analysis of the ϕ and ω-meson production is described in Section 3. The results of the measurements of different $\bar{p}d$ annihilation channels with pions in the final states are discussed in Section 4. Production of Λ hyperons is discussed in Section 5. Section 6 contains the concluding remarks.

2 Experimental apparatus, trigger and data taking

2.1 The OBELIX spectrometer

The measurements were performed using the OBELIX spectrometer on the M2 beam line at the CERN Low Energy Antiproton Ring (LEAR). The layout of the OBELIX spectrometer is shown in Fig.1. The full description of the OBELIX spectrometer can be found elsewhere [18]. Here we give only a short description of the detectors relevant to the present measurement.

The OBELIX spectrometer consists of four sub-detectors arranged inside and around the Open-Axial Field Magnet (OAFM), providing a field of 0.5 T in an open volume of about 3 m^3 . These detectors are:

1) the Spiral Projection Chamber (SPC) : an imaging vertex detector with three-dimensional readout for charged tracks and X-rays detection;

2) the Time-Of-Flight (TOF) system: two coaxial barrels of plastic scintillators for charged particle identification at the trigger level. The first barrel consists of 30 slabs (1 cm thick, 80 cm long) situated 18 cm from the beam axis, the second barrel consists of 84 slabs (4 cm thick, 300 cm long) located 136 cm from the beam axis. The intrinsic time resolution of the system is 800 ps FWHM;
3) the Jet Drift Chamber (JDC) for tracking and particle identification by dE/dx measurement. The detector consists of two half-cylinders (160 cm in diameter, 140 cm long). The 3280 sense wires are organized into 82 azimuthal sectors of 4^0 and are equipped with a 100 MHz 8 bit FADC readout system on both sides. The intrinsic spatial resolution is $\sigma_z = 12$ mm, $\sigma_{r,\phi} = 200$ μm. The momentum resolution, which was measured at 928 MeV/c for monoenergetic pions from the reaction $\bar{p}p \rightarrow \pi^+\pi^-$, was found to be $\sigma = 3.5\%$.
4) the High Angular Resolution Gamma Detector (HARGD): an electromagnetic calorimeter consisting of four modules made by layers of 3x4 m^2 lead converter foils enclosed by planes of limited streamer tubes.

The HARGD modules were under test during the data acquisition and their data are not included in this analysis.

2.2 Data taking and trigger configuration

Antiprotons of 105 MeV/c supplied by LEAR with $\Delta P/P < 10^{-3}$ crossed a 80 μm beam scintillator counter, which gave the start to the event timing and trigger logic. After passing through the 78 μm mylar entrance window the antiprotons were stopped in a cylindrical gaseous target filled with deuterium at NTP. The thickness of the target mylar walls was 12 μm. The length of the target was 62 cm and the antiprotons stopped in a rather limited central part of the target.

The diameter of the target was 6 cm and to avoid the problems connected with the annihilation on the target mylar walls the trigger signal was generated in a way which took into account the fact that signals in the inner TOF slabs from annihilation in gas arrived later in time then those from the annihilation in mylar.

To suppress the annihilations in mylar all read-out systems of the OBELIX detectors were active only within a time gate which arrived 20 ns after the signal of the front beam scintillator. The width of the time gate was 16 ns. The effect of this time selection is shown in Fig.2. In Fig.2a the distribution of the minimum times in the inner TOF slabs for the annihilation events with different z-coordinates of the vertex is reported. One can see two spots in this plot , which can be separated by a straight line: one, at small times, from annihilation on mylar, and the other, with typical time $t > 20$ ns, from annihilation in the target gas. These two regions can be well separated by the projection on the straight line. The projection on this line gives the distribution shown in Fig.2b by the dashed line. One can see two peaks, the small one coming from the annihilation on mylar and the big one from the annihilations in the target gas. The solid line shows the distribution of the annihilation times occurring only within the 16 ns gate signal. The bump from the annihilations on mylar practically disappears. Only small part of the annihilations on mylar still contaminates the data sample. This contamination was estimated as $W(myl) = (0.60 \pm 0.02)\%$ of all annihilations.

The distribution of the annihilation vertices along the beam axis is shown in Fig.2c. The dashed line corresponds to the distribution without demand on the time gate, the solid line is the z-distribution of the vertices within the time gate of 16 ns. It is seen that the selection of the events within the gate indeed chooses the annihilations in the central part of the target. This distribution also demonstrates that practically all events are due to annihilations at rest;

the percentage of annihilations in flight was determined as $W(in\ flight) = (0.80 \pm 0.03)\%$. The part of the annihilations in the front mylar window was $W(front) = (0.04 \pm 0.02)\%$.

The data used in this analysis were collected with a special trigger dedicated to the selection of two charged kaons from ϕ decays. The trigger conditions were as follows:

1. Three or four hits in inner and outer layers of the TOF system.
2. Angular correlations.

The topology of the trigger was chosen after Monte Carlo simulation of the reaction

$$\begin{aligned} \bar{p} + d \ &\rightarrow \ \phi + \pi^- + p_s \\ &\phi \rightarrow K^+ + K^- \end{aligned}$$

It turned out that in the lab system the opening angle between two kaons was rather small, $\approx 25 \pm 13^0$, whereas the angle between the pion and a kaon was rather large, $\approx 179 \pm 19^0$. So a typical event looked like a pion recoiling back-to-back off a pair of strongly correlated kaons.

To select events with such angular correlations the following coincidence between the signals from the counters of the inner TOF barrel was requested: two hits in any three adjacent slabs correlated with one hit in an opposite slab.

3. Demand on a slow particle.

To increase the percentage of kaons among the triggered events it was requested that the time difference between any hit in the inner TOF counters and a hit with maximum time in the outer TOF barrel should be greater than 9 ns. This condition rejected pions which had average time difference of the order of 3 ns.

The overall statistics consisted of $1.1 \cdot 10^6$ events with trigger. A sample of $1.4 \cdot 10^5$ events with the minimum bias trigger, requiring only the disappearance of an antiproton in the target, and $1.8 \cdot 10^5$ events with trigger on multiplicity (from 3 to 8 hits in the TOF barrels) was also available.

2.3 Trigger efficiency

The trigger efficiency was evaluated from the sample of the minimum bias events. These events were recorded with the special flags, corresponding to conditions 1-3 used in the trigger. The data were then analyzed in order to determine the sample of events which did obey the trigger conditions. Comparison of this sample with the sample of the flagged events gave the trigger efficiency. This information was inserted in the Monte Carlo simulation code.

The efficiencies of the inner and outer TOF counters were also determined from the analysis of the minimum bias data. A map of the efficiency of each slab of the TOF system was constructed and used in the Monte Carlo code. The average efficiency of the inner TOF counters turned out $\epsilon(tof) = (93 \pm 1)\%$ for one track. For the outer layer of TOF, $\epsilon(TOF) = (88 \pm 1)\%$.

2.4 Evaluation of the total number of annihilations

The total number of annihilations in the target was measured using the inner TOF barrel of scintillator counters. The system counted first the number of hits N_0 in the barrel within the time gate. If within the gate the trigger requirements were fulfilled, the event acquisition started. All the counter scalers were inhibited during the readout of an event. If another antiproton hitted the beam counter in a time interval of the readout, a signal of the pile-up stopped the event acqusition. So the total number of annihilations N_M which occurred in

the detector when it was open for data taking was:

$$N_M = N_0 \frac{N(events)}{N(trig)}(1 - W(myl) - W(in\ flight) - W(front))\frac{1}{\epsilon_M} \qquad (11)$$

were $N(trig)$ is the number of all triggers, $N(events)$ is the number of readout events undisturbed by the pile-up antiprotons, $W(myl)$, $W(in\ flight)$ and $W(front)$ are the corrections for annihilation in the mylar walls, in-flight and in the front target window, respectively.

The quantity ϵ_M is the efficiency of the inner barrel of TOF for the monitoring procedure. The losses include annihilations into neutral final states, events with undetected charged particles due to the geometrical acceptance of the barrel and the efficiency of the TOF counters. It turned out that $\epsilon_M = 0.982 \pm 0.004$.

3 ϕ and ω meson production

We have analysed the reactions of antiproton annihilation in deuterium for two regions of proton momenta: $P < 200$ MeV/c and $P > 400$ MeV/c. The main motivation to choose the region of low energy protons was the intention to obtain branching ratios for the annihilation on neutron. It was found in previous experiments with bubble chambers [7],[8] that the distribution of the proton-spectators with $P < 200$ MeV/c followed a Hulthen-like spectrum, which means that the effects of meson rescattering were small in this region.

The limit of $P > 400$ MeV/c was chosen since it is starting from this momentum value that the experimental conditions for detecting protons in the OBELIX apparatus become optimal. Indeed, protons with lower momenta have a significant probability to interact with the material of the inner TOF barrel, which is 1 cm thick.

3.1 $\bar{p} + d \longrightarrow \pi^- + \phi + p_{spectator}$

ϕ-mesons were searched looking for their decays into K^+K^-. The events with 3 tracks in JDC and negative total charge were analyzed. To select the final state 1C kinematic fit was performed and events with C.L. >5% were accepted for further analysis.

To separate kaons from pions a cut on time-of-flight was applied. In Fig.2d the β distribution of the particles passing through the above mentioned cuts is shown. The band of kaons is clearly visible. Solid lines correspond to the band used for kaon selection.

To choose events with proton spectators, a cut on the total momentum of the charged particles in JDC, $P_{tot} < 200\ MeV/c$, was introduced.

In Fig.3a the invariant mass of the K^+K^- system for events satisfying all selection criteria is shown. A clear narrow peak in the ϕ region is seen, superimposed on some background. The distribution was fitted with a Breit-Wigner function smeared by a gaussian:

$$F(m) = BG(m) \cdot (1 + c_0 \cdot BW'(m)) \qquad (12)$$

where m is the invariant mass of two kaons and

$$BW'(m) = \int BW(m', m_\phi, \Gamma_\phi) \cdot G(m')\, dm' \qquad (13)$$

Here

$$BW(m', m_\phi, \Gamma_\phi) = \frac{\Gamma(m')}{(m_\phi - m')^2 + \Gamma(m')^2/4} \qquad (14)$$

is the Breit-Wigner function with the width

$$\Gamma(m') = \Gamma_\phi \left(\frac{q(m')}{q(m_\phi)}\right)^3 \frac{m_\phi}{m'} \tag{15}$$

smeared by the gaussian $G(m')$ which reflects the experimental mass resolution:

$$G(m') = (\sqrt{2\pi}\sigma)^{-1} \cdot exp(-(m - m')^2/2\sigma^2) \tag{16}$$

$q(m)$ in (15) being the kaon momentum in the resonance rest frame.

The background was approximated by the following expression

$$BG(m) = (m - m_0)^{a_1}\ exp(a_2 + a_3 m + a_4 m^2) \tag{17}$$

where m_0 is the threshold value from which the invariant mass of the K^+K^- system is started, and a_i are free parameters.

The data were fitted integrating the expression (13) in each bin of the experimental histogram. The width of ϕ was fixed from the Particle Properties Tables [6].

The parameter σ of gaussian (16), which corresponds to the experimental mass resolution, is $\sigma = 4.1 \pm 0.2\ MeV$.

There were 859 ± 57 events under the ϕ peak.

3.1.1 Reliability of the ϕ selection

The trigger on a slow particle and strong angular correlations turned out to be quite adequate for selection of the $\phi\pi^-$ final state. To illustrate this in Fig.4a the invariant mass of kaon pairs is plotted for events passing through the kinematical fit cut and TOF identification as $K^+K^-\pi^-$ final state. Remember that the trigger should select events with configuration 1-(23), where particle 1 is back-to-back to a pair of strongly correlated particles 2 and 3. In the case of the ϕ decay we expect that particles 2 and 3 should be kaons. Whereas for the non-resonant $K^+K^-\pi^-$ channel two kaons may occur in all combinations (13),(23) and (12).

The open histogram in Fig.4a corresponds to the sum of all three combinations (13),(23) and (12), the hatched part of the histogram corresponding to the "wrong" combinations (13) and (12). One can see that the ϕ peak is clearly dominating only in the right combination (23), and there is no contamination from the "wrong" combinations in the ϕ-meson region. It means that we could correctly assign the masses of the particles, in some sense, already at the trigger level.

In principle, it is possible to have some contamination from the channel

$$\bar{p} + d \longrightarrow \pi^- + \pi^- + \pi^+ + p_s \tag{18}$$

because its branching ratio is two of magnitude orders greater than that for the $\phi\pi$ channel. To estimate the contamination from reaction (18) we plotted the value of χ^2 for the hypothesis (18) for events that passed through the selection criteria for identification of the $KK\pi$ final state. In Fig.4b the χ^2 for the hypothesis (18) is plotted versus the K^+K^- invariant mass. The solid line shows the 5% C.L. for the hypothesis 3π, i.e. events below this line may be regarded as belonging to reaction (18). One can see that there are no events in the region of the ϕ mass. From this one can conclude that the background consists only of $KK\pi$ events and the chosen cuts provide reliable suppression of the 3π channel (18).

3.1.2 Comparison with the Monte Carlo simulation

In Fig.5 the momentum distributions of pions, kaons and "proton-spectators" as well as the distribution on the missing mass for events that passed the selection criteria are compared with results of the Monte-Carlo simulations (shown by crosses). The momentum distribution of negative pions (Fig.5a) has a maximum at 650 MeV/c, as expected from the kinematics of the $pn \rightarrow \phi\pi^-$ binary reaction. The Fermi motion of the neutron in the deuteron smears the momentum of pions and the final distribution may be approximated by a gaussian with $\sigma = 27.5 \pm 1.3\ MeV/c$.

In Fig.5b the momentum distribution of kaons is shown. The average kaon momentum is around 350 MeV/c, i.e. the kaons are slower than pions. This facilitates the selection of kaons from pions by TOF.

In Fig.5c the distribution of the total momentum of particles in JDC $\vec{P}_{tot} = \vec{p_1} + \vec{p_2} + \vec{p_3}$, which should be equal to the momentum of the proton-spectator, is shown. Indeed, the P_{tot} distribution exhibits the typical Hulthen-like behavior and it practically coincides with the distribution obtained by the Monte-Carlo simulation shown by crosses. In the Monte-Carlo simulation the Locher-Svarc [19] deuteron wave function was used.

In Fig.5d the missing mass squared distribution is shown for the reaction $\bar{p}d \rightarrow \phi\pi^- X$. A clear bump at the proton mass can be seen. It is worthwhile to mention that the background reaction

$$\bar{p} + d \longrightarrow \phi + \pi^- + \pi^0 + p_s \tag{19}$$

should have the MM^2 starting at $1.16\ GeV^2$. The absence of events in this region indicates that the selection criteria work well in suppressing this background reaction.

3.1.3 Angular distribution of kaons from ϕ decay

One of the interesting features of the strong violation of the OZI rule in antiproton annihilation is the observation made by the ASTERIX group [2] that the yield of the $\phi\pi$-channel is substantial if the annihilation takes place from the S-wave in protonium. For the annihilation from P-wave they have not seen the $\phi\pi$ channel at all.

In present data the angular distribution between a kaon and the direction of ϕ is fairly well described by $\sin^2\theta$ (see Fig.6), as expected for annihilation from the $^3S_1$ initial state. The annihilation from the $^1P_1$-state would lead to a uniform angular distribution.

However the apparent absence of annihilation into $\phi\pi^-$ from the P-state should not be regarded as the indication of small branching ratio for $\phi\pi^-$ in this initial state. In spite of the fact that the probability for the antiproton to annihilate from S- and P-wave of the $\bar{p}d$ atom is believed to be almost equal in deuterium gas [2], the probabilities to annihilate from the $(\bar{N}N)$ S- and P-waves may be different. The antiproton in deuterium from a fixed atomic state may annihilate in nucleon-antinucleon states with different angular momenta. Indeed a previous OBELIX result [20] indicated that the percentage of annihilation from the $(\bar{N}N)$ P-wave in gaseous deuterium is $(18 \pm 7)\%$ and theoretical estimations [21] give the value of $\simeq 33\%$ for the $(\bar{N}N)$ P-wave fraction in deuterium . Therefore the angular distribution of Fig.6 may simply reflect the S-wave dominance of $(\bar{N}N)$ interaction in $\bar{p}d$ annihilation.

3.2 $\bar{p} + d \longrightarrow \pi^- + \phi + p_{fast}$ $(P_p > 400 MeV/c)$

To select this reaction in the high momentum proton region $(P > 400 MeV/c)$ the sample of events with 4 tracks in JDC was used, having the confidence level for the hypothesis greater than 3% and obeying time-of-flight cuts for protons and kaons.

The invariant mass distribution of K^+K^- for events passing through the applied cuts is shown in Fig.3b. The statistics is rather scarse but the peak from ϕ meson is seen clearly. There are 38 ± 6 events under the peak.

The Monte Carlo simulation of this reaction is complicated by the fact that one should know the behaviour of the proton momentum distribution at rather high momenta. It is impossible to use simply some realistic deuteron wave function, because rescattering of the annihilation mesons strongly distorts the high momentum tail of the proton spectrum [21]. In the present simulation the results of the calculations by B.S.Zou and M.P.Locher, where different meson rescattering diagrams were considered [22], were used.

The interest in measuring the ϕ yield at high proton momenta was motivated by the suggestion [23] to look for the exotic C(1480) resonance production in the binary reaction

$$\begin{aligned} \bar{p} + d \longrightarrow \quad & C(1480)^- + p \\ & C^- \rightarrow \pi^- + \phi \end{aligned} \tag{20}$$

as a possible explanation for the OZI-rule violation.

This controversial exotic state with $I = 1, J^{PC} = 1^{--}$ and width $\Gamma = 130 \pm 60$ MeV was found by the Lepton-F group [24] and was regarded as a candidate for the 4-quark $ssqq$ state [25], [26].

In Fig.7 the invariant mass distribution of $\phi\pi^-$ is plotted for the raw data (a) and for the data corrected for the experimental acceptance (c). The behavior of the acceptance of the apparatus is given in Fig.7b. A peak at about 1.5 GeV can be seen, but the scarcity of the statistics prevents any conclusions.

3.3 $\bar{p} + d \longrightarrow \pi^- + \omega + p_{spectator} \quad (P_p < 200 MeV/c)$

To test the OZI-rule it is desirable to compare the measurements of the ϕ and ω-meson yields under the same experimental conditions. However for the present trigger, dedicated to the selection of events with at least one slow particle in the final state, the $\bar{p}+d \rightarrow \pi^-+\omega+p_{spectator}$ channel was not suitable. In fact, the proton-spectators could not pass through the inner barrel of the TOF system and the pions in this reaction are mainly fast. On the other hand, there were no measurements of this reaction for annihilation in gas. So the sample with only the multiplicity trigger was used to determine the branching ratio of this reaction.

To select the reaction events with 3 tracks in JDC and the proper total charge were chosen. Information from the vertex detector SPC was also used in the cases when it registered a particle with positive charge and with a track which was not connected to any other tracks in JDC.

The background reactions

$$\bar{p} + d \longrightarrow 2\pi^- + \pi^+ + m\pi^0 + p_s \qquad \text{m=0 or 2,3...} \tag{21}$$

were suppressed by the cuts on the missing mass.

For further elimination of the background the kinematical features of the binary reaction $\bar{p}n \rightarrow \pi^-\omega$ were taken into account, accordig to which a π^- recoiling against a ω should have a momentum around 750 MeV/c. At the same time the momenta of positive pions from ω decay are less than 700 MeV/c. This fact gives the possibility of rejecting background events with low momenta π^- and high momenta π^+. Following the Monte Carlo simulation cuts on π^- momentum $P > 600\ MeV/c$ and on π^+ momentum $P < 600\ MeV/c$ were chosen.

In Fig.3c the invariant mass of the $\pi^+\pi^-\pi^0$ system for events obeying the selection criteria is plotted. To calculate the neutral pion momentum it was assumed that

$$\vec{P}_{\pi^0} = -\vec{P}_{tot} \tag{22}$$

where $\vec{P}_{tot}$ is the total momentum of pions and of the proton-spectator measured by SPC.

A peak corresponding to ω production can be seen; however, the assumption (22) to determine the π^0 momentum via the total momentum of pions and proton-spectator is not quite perfect. In fact, approximately 30% of proton-spectators have low momenta ($P < 40$ MeV/c) and they simply can not pass through the mylar of the target to enter into the vertex detector. This eventually increases the smearing of the ω peak due to the summing up of errors in the determination of the charged particle momenta.

The distribution of Fig.3c was fitted by the sum of a gaussian and a third-order polynomial. The number of ω's in the peak turned out to be $N_\omega = 222 \pm 39$.

3.4 $\bar{p} + d \longrightarrow \pi^- + \omega + p_{fast} \quad (P_p > 400 MeV/c)$

For selection of this reaction in the high momentum proton region ($P > 400$ MeV/c) the data from the trigger sample, with 4 tracks in JDC, were used having the 1C fit confidence level at least 3%, with protons identified by the time-of-flight.

The invariant mass distribution of the $\pi^+\pi^-\pi^0$ system for these events is shown in Fig.3d. A clear peak in the ω region can be seen. The distribution was approximated by a gaussian with a third order polynomial. There are 499 ± 63 events under the peak. The width of the peak is $\sigma = 21 \pm 8$ MeV. The mean value is $m = 782.0 \pm 3.1$ MeV. It is remarkable that the position of the ω peak is not changed.

To perform the Monte Carlo simulation one has to deal with the same problem of the determination of the high momentum tail of the proton spectrum. Fortunately, the statistics of the ω's allowed to divide the proton momentum spectrum in bins of 100 MeV/c width and find the number of ω's in each bin. These numbers were corrected for the acceptance of the apparatus assuming a flat dependence of the proton momentum distribution within each bin. The resulting dependence of the ω yield from the proton momenta is shown in Fig.8. One can see that it is rather flat. The solid line corresponds to the result of the calculations by F.Lev and D.Buzatu [27], where rescattering of the annihilation mesons was taken into account. Experimental data are slightly higher than the prediction of the meson rescattering model, but the momentum dependence is reproduced rather well.

3.5 ϕ and ω branching ratios

The final results on ϕ and ω production, for different regions of the proton momentum, are collected in Table 1, where number of events, detection efficiencies ϵ and branching ratios are given. The detection efficiency for the total procedure of final state selection was determined by Monte Carlo simulations. It took into account the geometrical acceptance, the trigger efficiency as well as the selection cuts used. The correction for the neutral modes of ϕ and ω decays was included in the branching ratios shown in Table 1.

There are some systematic errors in the procedure adopted for the determination of the branching ratios. The following effects were analysed:

1. The efficiencies of the counters of the TOF system were included into the Monte Carlo procedure by a map obtained from the events of the minimum bias sample. The procedure of determination of such a map has some uncertainties, reflecting, for instance, differences between the map for pions and for kaons due to different dE/dx. The estimated systematic error is $\epsilon_1 = ^{+5}_{-16}$ %.

2. Uncertainties in the Monte Carlo procedure in taking into account nuclear interactions of the particles. It results in an increasing of the branching ratios of 2%, i.e. $\epsilon_2 = +2\%$.

3. Uncertainties in the determination of the vertex leads to slightly different distributions for experimental data and Monte Carlo data. The corresponding systematic error is $\epsilon_3 = -0.5\%$.

The total systematic error including all the above effects is $\epsilon_{sys} = ^{+5.4}_{-16}$ %.

It was not possible to separate the annihilation on proton and on neutron in deuterium. That is why the branching ratios of Table 1 concern all annihilations in deuteron. However, in the case of low proton momenta ($P < 200\ MeV/c$) the information of [28], according to which the ratio between annihilation on neutron and on proton was $R(\bar{p}n/\bar{p}p) = 0.81 \pm 0.03$ was used. Based on this proportion it was possible to obtain from the present data the branching ratios of ϕ and ω production in antiproton-neutron annihilation. They are given in the last row of Table 1.

Even though the straightforward comparison with the results of the measurements in bubble chambers [7],[8] is not quite correct, it is nevertheless useful to recall that $B.R.(pn \to o\pi^-) = (9.2 \pm 1.1) \cdot 10^{-4}$, [7], $B.R.(\bar{p}n \to \phi\pi^-) = (8.8 \pm 2.2) \cdot 10^{-4}$, [8].

The present statistics is a factor of 10 greater than that in these experiments.

The old values for $B.R.(\bar{p}n \to \omega\pi^-)$ from the measurements in liquid deuterium are: $B.R.(pn \to \omega\pi^-) = (6.7 \pm 1.1) \cdot 10^{-3}$, [9], $B.R.(\bar{p}n \to \omega\pi^-) = (4.1 \pm 0.8) \cdot 10^{-3}$, [10], in disagreement with the present results. These bubble chamber results are also in disagreement with the branching ratio $\bar{p}p \to \omega\pi^0$ which has recently been measured by the Crystal Barrel Collaboration [29]. The advantage of the CB measurements is that they have directly measured all γ's from the ω decays. They found $B.R.(\omega\pi^0) = (5.73 \pm 0.47) \cdot 10^{-3}$. According to the isospin invariance, $B.R.(\omega\pi^-) = 2 \cdot B.R.(\omega\pi^0)$.

In order to test the whole procedure of the determination of the branching ratios, the branching ratio of the reaction

$$\bar{p} + d \longrightarrow 2\pi^- + \pi^+ + p \tag{23}$$

were evaluated both for the data sample with trigger on ϕ and for the data sample with multiplicity trigger. Reaction (23) was selected for protons with momenta 0.4-0.8 GeV/c. The branching ratios turned out:

$$B.R.(\bar{p} + d \to 2\pi^- + \pi^+ + p) = (16.6 \pm 0.9) \cdot 10^{-4}, \quad \text{for } \phi\text{-trigger data} \tag{24}$$

$$B.R.(\bar{p} + d \to 2\pi^- + \pi^+ + p) = (16.3 \pm 1.7) \cdot 10^{-4}, \quad \text{for multiplicity trigger data} \tag{25}$$

This agreement between branching ratios obtained from different sets of data, with different monitor numbers and different trigger efficiencies, gives confidence to the whole procedure of the absolute B.R. evaluation.

3.6 Violation of the OZI-rule

From the data shown in Table 1 the following ratio R=$\phi\pi/\omega\pi$ was obtained

$$\begin{aligned} R\ (\phi\pi^-/\omega\pi^-) = \quad & (133 \pm 26) \cdot 10^{-3} \qquad P < 200\ \text{MeV/c} \\ & (113 \pm 30) \cdot 10^{-3} \qquad P > 400\ \text{MeV/c} \end{aligned}$$

These values are in agreement with the ratio $\phi\pi^+/\omega\pi^+$ obtained by the OBELIX collaboration using an antineutron beam [11] and they are considerably higher than the OZI predictions (2) $R = (0.15 - 4.2) \cdot 10^{-3}$.

Moreover, wishing to take into account the difference of the phase space for the $\phi\pi$ and $\omega\pi$ final states for annihilation on a quasi-free neutron ($P < 200 MeV/c$), one should multiply the

ratio R by the phase space factor $f = k_\omega/k_\phi = 1.18$, which increases the OZI-rule violation for $\bar{p}n$ annihilation.

It is worthwhile to evaluate the magnitude of the OZI rule violation introducing, following Okubo [30], the parameter Z of the OZI-rule breaking

$$Z = \frac{\sqrt{2}M(A+B \to C+s\bar{s})}{M(A+B \to C+u\bar{u}) + M(A+B \to C+d\bar{d})} \tag{26}$$

Here $M(A+B \to C+q\bar{q})$ are the matrix elements of the reaction of $q\bar{q}$ production in the interaction of non-strange hadrons A,B,C.

Then the ratio of the matrix elements of ϕ and ω production could be written as

$$\frac{M(A+B \to C+\phi)}{M(A+B \to C+\omega)} = -\frac{Z+\tan(\theta-\theta_i)}{1-Z\tan(\theta-\theta_i)} \tag{27}$$

The OZI-rule demands that $Z = 0$. The degree of validity of the rule has been verified in different experiments on πp, pp scattering or $\bar{p}p$ annihilation at different energies (see [1],[30]-[34]). Typically, the deviations from the OZI-rule give the following limit on Z:

$$|Z| \leq 0.06 - 0.10 \tag{28}$$

It means that in all hadronic interactions the OZI-rule is broken at most at the order of 6-10%, i.e. it could be regarded like a well established semi-empirical rule.

The present results on the ϕ/ω ratio, expressed in terms of the Z parameter, demonstrate, however, substantial violation of the OZI-rule:

$$|Z| \geq 0.29 \pm 0.03 \tag{29}$$

The same strong violation was found in the ASTERIX data [2] and in the recent Crystal Barrel results [3].

The reasons why just annihilation at rest is so particular among all other hadronic interactions deserve a separate study.

In order to explain this apparent violation of the OZI-rule in the antiproton annihilation several suggestions were put forward:

Resonances in the $\phi\pi$ system. If there is a resonance in the $\phi\pi$ system under the $\bar{N}N$ threshold, like for instance the controversial C(1480) meson [24], then it would be possible to explain (see, e.g., [26]) why the yield of $\phi\pi$ from the annihilation in ($\bar{\text{N}}$N) S-wave is large, while from the P-wave it is surprisingly small [2]. However, the substantial violation of the OZI-rule in the $\phi\gamma$ channel could not be due to the decay of the C-meson, which is a 1^{--} state. Direct searches for the C-meson in $\bar{p}p$ annihilation have been unsuccessful: the ASTERIX collaboration [2] did not observe the C-meson in the antiproton annihilation in a hydrogen gas target in the $\phi\pi^+\pi^-$ mode at the upper level of $3 \cdot 10^{-5}$. The Crystal Barrel collaboration has not seen the C-meson in annihilation in the hydrogen liquid target in $\phi\pi^0\pi^0$ channel [35] either. As for OBELIX search for the C-meson, the scarcity of available statistics prevents any firm conclusion (see Fig.7).

In [26] the isoscalar partner of the C-meson was also predicted, which should couple to $\phi\eta$ channel. However no OZI rule violation was seen in this mode [3].

Final state interaction of kaons. It is known (e.g. [3]) that the $\bar{K}K\pi$ final state dominates by the K^*K channel. It is tempting to assume [36] that the ϕ is produced

due to the final state interaction of two kaons formed in the OZI allowed process $\bar{p}p \to K^*K \to K\bar{K}\pi \to \phi\pi$. Specific calculations of the ϕ production in different channels have been made in [36],[37]. They underestimate the experimental branching ratios by at least a factor of 2. Moreover, as it was pointed out in [38], the rescattering model could not explain why the ratio $\phi\pi\pi/\omega\pi\pi$ is small, though the branching ratio for $K^*\bar{K}^*$ production is larger than that for $K^*\bar{K}$ production.

Admixture of the strange sea quarks in proton. It was proposed [32],[33] that the abundant ϕ meson production can be the consequence of an admixture of $\bar{s}s$ pairs in the nucleon. As a recent analysis [34] shows, an intrinsic strangeness contribution in the nucleon wave function of only few percent is enough to explain the existing violation of the OZI rule in $\bar{N}N$ annihilation at rest.

At first glance, the intrinsic strangeness of the nucleon should lead to the same enhancement of the ϕ production in all annihilation channels. That is contrary to the experimental data. The ASTERIX collaboration [2] measured the production of ϕX and ωX final states with $X = \pi, \eta, \omega, \rho, \pi\pi$ from S- and P-wave states of the protonium. It occurs that the experimental values of the ϕ/ω ratio R for different annihilation channels are slightly higher (by a factor of 2-3) than the OZI-rule predictions (2). The only exception is for the channel with $X = \pi$ for annihilation from the S-wave.

The measurements of the Crystal Barrel collaboration [3] also showed that the ratios of $\phi\pi\pi/\omega\pi\pi$ and $\phi\eta/\omega\eta$ only slightly deviate from the OZI prediction of (2).

An explanation of the different degree of the OZI rule violation in different channels of $\bar{p}p$ annihilation can be obtained under the hypothesis of a polarized strange sea in the nucleon [34]. According to this model, the quantum numbers of an $\bar{s}s$ pair formed from the nucleon strangeness component depend strongly on the spin of the initial state. The model predicts that the $\bar{s}s$ pairs with the quantum numbers of the ϕ-meson are produced mainly from the spin triplet states. The ϕ production from the spin singlet initial states should be suppressed. Indeed, as discussed above, the $\phi\pi$ channel could be formed either from $^3S_1$ or from $^1P_1$-state. The strong OZI-violation exists only in the spin triplet $^3S_1$ state.

Different experimental tests of this model were proposed [34]. This model could be tested by measurements of the $f_2'(1525)/f_2(1270)$ production ratio in P-wave annihilations and by experiments with polarized beams and polarized targets.

So the nature of the strong OZI-rule violation in the antiproton annihilation at rest is not yet clear. Obviously, a systematic study of annihilations into channels containing kaons is needed.

4 $\bar{p}d$ annihilation channels with pions in the final state

As a by-product of the studies of the ϕ-meson production, data on antiproton annihilation at rest with deuterium in the multiplicity (3-8) trigger were also taken. It was possible to select the following reactions:

$$\bar{p} + d \longrightarrow 2\pi^- + \pi^+ + p \tag{30}$$
$$\bar{p} + d \longrightarrow 2\pi^- + 2\pi^+ + n \tag{31}$$
$$\bar{p} + d \longrightarrow 3\pi^- + 2\pi^+ + p \tag{32}$$
$$\bar{p} + d \longrightarrow 3\pi^- + 3\pi^+ + n \tag{33}$$

in the region of nucleon-spectator momenta ($P < 200$ MeV/c).

These reactions were identified through a kinematical fit. In Fig.9 the distributions of the missing mass squared are shown. The solid lines correspond to the distributions when the nucleon-spectator cut of $P_{tot} < 200$ MeV/c was applied. The hatched histograms correspond to the events which have the confidence level for the investigated reactions greater than 10%. The peaks from the nucleon-spectator are seen clearly. The estimation of the background from the reactions with an additional π^0 gives the contaminations at the level of 10%, 2%, 1% and 1% for reactions (30)-(33), respectively.

The corresponding number of events, Monte-Carlo simulated detection efficiencies $\epsilon(MC)$ and branching ratios are given in Table 2. The branching ratios are normalised to the annihilation on proton or neutron in deuterium in the same manner as was discussed in Section 3.5.

From the results of Table 2 one can conclude that the present values for the branching ratios are in agreement with the results of the previous experiments. The present statistics is not large and it prevents a detailed amplitude analysis of the observed final states.

However the experiment offers the possibility of studying the formation of the same pion systems in different regions of proton momenta, which brings some new interesting information concerning the dynamics of pd-annihilation. The channel with 3 charged pions in the final state will be firstly considered.

4.1 $\bar{p} + d \longrightarrow 2\pi^- + \pi^+ + p$

This channel has been studied for two intervals of proton momenta $P < 200$ MeV/c and $P > 400$ MeV/c. In Fig.10 the invariant mass distributions of the $\pi^+\pi^-$ (solid line) and $\pi^-\pi^-$ (dashed line) systems are shown. Fig.10a corresponds to the annihilation with proton-spectators ($P < 200$ MeV/c), Fig.10b shows the dipion invariant mass distribution for annihilation with high-momenta protons ($P > 400$ MeV/c).

It is possible to see the well known pattern of the $\pi^+\pi^-$ invariant mass distribution with the peaks from ρ and $f_2(1270)$ meson decays. In the proton-spectator region (Fig.10a) a hint of a third bump at 1.5 GeV mass region also exists. The fit of this distribution with three Breit-Wigner functions and a third-order polynomial background gives the mass $M = 1538 \pm 20$ MeV for this enhancement.

A similar picture with an enhancement at 1565 MeV was observed by the ASTERIX collaboration in $pp \rightarrow \pi^+\pi^-\pi^0$ annihilation from P states of pp atom [43]. The Crystal Barrel collaboration saw this peak at slightly smaller mass (1515 MeV) in $\bar{p}p \rightarrow 3\pi^0$ [44]. The OBELIX collaboration also saw a bump at 1540 MeV in the annihilation of antineutrons $np \rightarrow \pi^+\pi^-\pi^+$ [45] . The nature and the quantum numbers of this state (or states) is the subject of hot discussions (see for review [46] and also [47]).

It is also interesting to compare the $\pi^+\pi^-$ distribution of Fig.10a with the corresponding one for the high-proton momentum region (Fig.10b). They are similar except for the absence of the bump at 1.5 GeV. The latter seems to be due to the obvious lacking of the phase space. The fit of the $\pi^+\pi^-$ distribution of Fig10b by two Breit-Wigner functions with a polynomial background shows that the position of the ρ and $f_2(1270)$ peaks do not differ from their known values (see also discussion in Section 4.3).

It is commonly assumed that the main source of the high momentum protons tail in pd annihilation is the rescattering of the annihilation mesons (see for instance, [21]). However, high momentum protons may be formed not only via meson rescattering (i.e. near on-shell meson-nucleon interaction) but also due to absorption of annihilation mesons in the so-called

Pontecorvo reactions (see [17],[18],[23] and references therein).

$$\bar{p} + d \longrightarrow M + N \tag{34}$$

Here M stands for any meson like η, ρ, ω or meson system of 2,3 ... pions. N is either a nucleon or a nucleon resonance like Δ or N^*.

The diagrams of the corresponding processes are shown in Fig.11. The relative contribution of the rescattering and the Pontecorvo reaction to the formation of the high momentum tail of the proton spectrum is not known a priori. But it is clear that the two processes should lead to different distributions of the $\pi^+\pi^-$ invariant mass.

Indeed if the final state

$$\bar{p} + d \longrightarrow 2\pi^- + \pi^+ + p \tag{35}$$

is due to the Pontecorvo processes (Fig.11b), then it may be described as pN annihilation into 4 pions followed by absorption of one pion.

If the proton in reaction (35) acquires high momentum due to rescattering, it means that there was annihilation into 3 pions followed by meson-nucleon on-shell interaction (see Fig.11a).

The $\pi^+\pi^-$ invariant mass distributions are different for $\bar{p}N \to 3\pi$ and $\bar{p}N \to 4\pi$ channels. Thus if the Pontecorvo reactions were the major source of high momenta protons, then the $\pi^+\pi^-$ spectrum should be dominated by ρ-meson production and should look like that of Fig.12a (see Section 4.2).

From the fact that the $\pi^+\pi^-$ distributions of Fig.10 are similar, irrespective of the proton momentum, one can conclude that the rescattering processes are dominant in the formation of the proton high-momentum tail up to 1 GeV/c.

4.2 $\bar{p} + d \longrightarrow 2\pi^- + 2\pi^+ + n$

The invariant mass distributions of the events from this reaction are shown in Fig.12. The $\pi^+\pi^-$ invariant mass is shown in Fig.12a by the solid line. It exhibits only a strong peak from the ρ-decays. About 20% of the reaction is going on via the $\rho\rho$ intermediate state. The dashed line corresponds to the $\pi^-\pi^-$ invariant mass distribution. It is rather monotonous, as expected. The $\pi^+\pi^+$ and $\pi^-\pi^-$ invariant mass distributions shown in Fig.12b practically coincide. It indicates the absence of acceptance distortions. The $\pi^+\pi^-\pi^\pm$ invariant mass is shown in Fig.12c. It is also rather smooth.

In general, these distributions are very similar to those observed in $\bar{p}p \to 2\pi^-2\pi^+$ annihilation in liquid hydrogen [48].

4.3 $\bar{p} + d \longrightarrow 3\pi^- + 2\pi^+ + p$

This channel is interesting from the point of view of searching for resonances decaying into 4π in the reaction

$$\begin{aligned} p + n \longrightarrow \quad & \pi^- + \quad X \\ & X \to 2\pi^+2\pi^- \end{aligned} \tag{36}$$

This reaction was studied in a series of experiments [39],[49]. A strong enhancement was found in 4π invariant mass at $M = 1477 \pm 5$ MeV, $\Gamma = 116 \pm 9$ MeV with $J^{PC} = 2^{++}$. It was dubbed as $\xi(1480)$.

The same strong enhancement had been seen in the bubble chamber data selected with a cut on the proton momentum ($P < 150 MeV/c$) [40]. However, the assignment of the

quantum numbers has been questioned by a recent re-analysis by Gasperc [41]. This author found that the best description of the data is obtained with the 0^{++} state with mass 1390 MeV and $\Gamma = 310$ MeV, decaying in $\rho\rho$ and $\sigma\sigma$, where $\sigma\sigma$ is the S-wave dipion interaction. In this kind of analysis the mass of the resonance is lower than the mass of the observed peak, due to the interference of these two decay modes.

The OBELIX Collaboration [50],[51], and, more recently, Crystal Barrel Collaboration [52], repeated this analysis for the $\bar{n}p \to 3\pi^-2\pi^+$ channel and the $\bar{p}p \to \pi^+\pi^-3\pi^0$ channel, respectively. As in the Gaspero analysis the scalar quantum numbers seem to be preferential and the resonance parameters are $(M,\Gamma) = (1345,398)$ MeV and $(M,\Gamma) = (1374,375)$, respectively.

The ASTERIX collaboration studied reaction (36) and confirmed the existence of a strong peak in the 4π invariant mass [13]. The position of the peak strongly depended on the momentum of the proton. For example, for the data sample with an average proton-spectator momentum $< P >= 100$ MeV/c, the peak parameters were $(M, FWHM) = (1504,206)$ MeV , whereas for high momentum protons with $< P >= 400$ MeV/c the parameters are $(M, FWHM) = (1359,262)$ MeV.

ASTERIX data were selected without kinematical fit analysis and there were as many as 30% of background reactions with additional π^0's [13]. That background contribution may be the reason for the peak shifting.

The distributions of 4π invariant masses are shown in Fig.13. To select this reaction kinematical fit analysis and a cut on total momentum $P_{tot} < 200$ MeV/c were used. The solid line in Fig.13a shows the invariant mass distributions of the $2\pi^+2\pi^-$ system. It exhibits a strong peak at the 1.5 GeV region. The dashed line in Fig.13a corresponds to the invariant masses of the $\pi^+3\pi^-$ system, which may be regarded as a background. The difference spectrum obtained after subtraction of the background $3\pi^-\pi^+$ from the $2\pi + 2\pi^-$ distribution is shown in Fig.13b . The fit of this peak by a gaussian gives the following resonance parameters: $M = 1497 \pm 8$ MeV and $FWHM = 177 \pm 14$ MeV.

It is interesting to look at the scatter plot of Fig.13d , where the invariant masses of the dipions $\pi^+\pi^-$ are plotted. It is possible to see an accumulation of events just at the intersection of the two ρ bands. The ρ bands themselves seem to be absent. So it appears a dominance of the $\rho\rho$ mode in the decay of the resonance. The same picture was seen in antineutron-proton annihilation [51].

In order to select the channel (36) in the high momentum proton region, a sample of 6 prong events was analysed. Protons were identified by the TOF information and reaction (36) was selected by the kinematical fit. The invariant mass distribution of the $2\pi^+2\pi^-$ system is shown in Fig.13c. One can see that the peak in this distribution is indeed shifted towards low masses in comparison with the same distribution for the proton-spectator region (Fig.13a).

It is interesting to note that the Monte Carlo simulation of the reaction (36), under the assumption of a flat behavior of the proton momentum spectrum at high momenta, confirms the effect of the shifting of the peak position. In Fig.14a the result of the Monte Carlo simulation of the reaction (36), when a resonance with mass M = 1480 MeV and width $\Gamma = 260$ MeV decays into 4π system is shown. The assumption about flat proton momentum distribution for P>400 MeV/c, used in this simulation, leads to such a shrinkage of the available phase space, so that only a part of the broad peak structure survives. This induces an apparent shift of the peak in the 4π invariant mass distribution and a shift of the peak in the difference spectrum. The difference spectrum of the 4π system for the high proton momenta is shown in Fig.14b by the dashed line. Indeed, the peak position is shifted of almost 100 MeV downward in comparison with the same bump in the proton-spectator sample with

$P_{tot} < 200$ MeV/c (solid line).

In Table 3 the positions of different states seen in present data are shown for two regions of proton momenta. The positions of resonances like $\omega, \rho, f_2(1270)$ do not depend on the value of the proton momentum. At the same time, the broad bump in 4π invariant mass ($\xi(1480)$) changes its position if the energy of proton-spectator increases. An explanation of the shift of $\xi(1480)$ was given in [53] based on the assumption that rescattering of pions from the $\xi(1480)$ decays can distort the peak position. Indeed such rescattering could provide the flat proton momentum distribution which, as demonstrated by the Monte Carlo simulation, is the phenomenological reason for the shift of a broad structure as the $\xi(1480)$. Why such distortions do not occur with ordinary meson resonances is an open problem.

4.4 Δ-resonance excitation in $\bar{p}d$ annihilation

In Section 4.1 it was pointed out that the invariant mass spectra of $\pi^+\pi^-$ look rather similar for two regions of proton momenta: in proton-spectator region ($P < 200\ MeV/c$) and for high proton momenta $P = 400 - 800\ MeV/c$. This gives an indirect indication of the dominance of rescattering of annihilation mesons in the formation of the high momentum tail of the proton spectrum. But if pions do interact with the proton-spectator, then one should observe well-known features of πN interaction, such as the excitation of Δ resonances. Previous experiments on $\bar{p}d$ annihilation could not see these effects in the πp invariant mass distribution [54]. The sample with the multiplicity trigger was enriched with high momentum protons. Low energy protons (with P< 400 MeV/c) have a significant probability to interact with the material of the inner TOF barrel, which is 1 cm thick, and do not provide the trigger, being unable to reach the outer TOF barrel.

In Fig.15 the invariant mass distributions of π^+p (a) and π^-p (b) systems are shown. To increase the statistics, events from the inclusive channel

$$\bar{p} + d \longrightarrow \pi^+ + 2\pi^- + p + m\pi^0, \quad \text{m=0,1,2...} \tag{37}$$

were also selected. Protons and π^+ mesons were identified by the TOF information. Protons with momenta P> 400 MeV/c were selected.

The peak from the Δ^{++} resonance is clearly seen in Fig.15a, whereas the π^-p invariant mass distribution (Fig.15b) looks rather smooth. The fit of the π^+p distribution by a Breit-Wigner and a polynomial background gives the following resonance parameters: $M = 1220 \pm 4$ MeV, $\Gamma = 73 \pm 20$ MeV.

An evaluation of the effective mass spectra of πp systems in $\bar{p}d$ annihilation has been performed in [55]. It was predicted that the Δ peak should be seen in π^+p system whereas the excitation of Δ in the π^-p system is not so pronounced and smeared by rescattering. The results in Fig.15 confirm these predictions.

Another manifestation of strong meson rescattering can be seen from the behaviour of the proton momentum distribution in various exclusive channels. In Table 4 the branching ratios of the following reactions

$$\bar{p} + d \longrightarrow \pi^- + \omega + p \tag{38}$$

$$\bar{p} + d \longrightarrow 2\pi^- + \pi^+ + p \tag{39}$$

are given for different values of the proton momentum.

One can see that the branching ratios for both reactions are practically not changed with the proton momenta in the $P = 0.4 - 0.8$ GeV/c interval. This is in sharp contrast with the behaviour which is expected if the proton momentum distribution is determined by the

deuteron wave function only. For the $\omega\pi^-$ channel the dependence on the deuteron wave function is shown in Fig.8 by the dashed line.

Another interesting information is obtained from the comparison of the branching ratios of different channels in two regions of proton momenta (see Table 5).

It seems that the branching ratios of all investigated reactions decrease with proton momenta practically by the same factor. This feature is not so obvious. At first glance, the probability of the final state interaction for the channel with 5π should be greater than that for the $\phi\pi$ final state. However this probability also depends on the average momentum of pions and model calculations are needed to verify the observed "scaling".

5 Subthreshold production of Λ-hyperons

Antiproton annihilation on nuclei is an effective source of Λ hyperon formation (for a review, see [14]-[17]). Normally, in the annihilation on a free nucleon, Λ's are produced in the reaction $pp \to \Lambda\Lambda$ which has a threshold at $p_{th} = 1436$ MeV/c. However, in antiproton annihilation on nuclei even antiprotons at rest could create Λ via rescattering of the annihilation mesons. In this sense subthreshold Λ production is the unique possibility for the investigation of meson rescattering.

The Λ production in pd annihilation was studied in the bubble chambers [56] and in the ASTERIX experiment [57]. The statistics for the inclusive Λ production in these measurements was on the level of 400 and 700 events, respectively.

In this experiment Λ's were searched in the data sample obtained with the ϕ-meson trigger in the invariant mass of the $p\pi^-$ system. The protons were selected by the TOF information. The following channels were selected:

$$p + d \longrightarrow \Lambda + X \tag{10}$$

$$\bar{p} + d \longrightarrow \Lambda + K^+ + \pi^- \tag{11}$$

$$p + d \longrightarrow \Lambda + K^+ + \pi^- + \pi^0 \tag{12}$$

5.1 Inclusive production

In Fig.16a the invariant mass distribution of $p\pi^-$ pairs is shown. The peak in the invariant mass range of Λ contains 667 ± 78 events. It was fitted by a gaussian obtaining the following parameters: $M = 1115.5 \pm 0.5$ MeV and $\sigma = 3.5 \pm 0.4$ MeV.

To obtain the momentum spectrum of Λ a background spectrum from the events in the peak region was subtracted using the neighbouring bins in the invariant mass distribution of $p\pi^-$ pairs. The resulting distribution is shown in Fig.16b. The absence of low momentum Λ's is due to the fact that protons with momenta $P > 400$ MeV/c were selected.

The fit of this spectrum by a Maxwell-Boltzmann distribution is also shown in Fig.16b.

The main distinction between these data and the previous ones is that in this case one deals with a high momentum tail of the Λ spectrum at $P > 600$ MeV/c, whereas in the bubble chamber data [56] the soft part of the spectrum was measured. This feature is particulary suitable for the studies of the reactions (41)-(42) which are characterized by high momentum distribution of Λ's.

5.2 $\bar{p} + d \to \Lambda + K^+ + \pi^-$

To select this channel the following cuts were applied:

1. Total charge equals to zero.

2. Cut on the time-of-flight to select kaons and protons.

3. Confidence level for this hypothesis at least 5%.

In Fig.16c the invariant mass of the $p\pi^-$ system for the events that passed all selection criteria is shown. In the mass region of Λ a clear narrow peak is present. This distribution was fitted with the sum of a gaussian and a polynomial function. There are 35 ± 7 events in the peak. The parameters of the gaussian are $M = 1116.6 \pm 0.6$ MeV and $\sigma = 3.1 \pm 0.5$ MeV.

To study the contamination from other channels the following reactions were simulated: $pd \to \Lambda K^+\pi^-\pi^0$, $pd \to \Lambda K^+\pi^-2\pi^0$, $pd \to \Lambda K^+\pi^+2\pi^-$, $pd \to \Lambda K^0_L\pi^+\pi^-$, $pd \to \Lambda K^0_L\pi^+\pi^-\pi^0$ and $pd \to \Lambda K^0_S\pi^0$.

Taking into account their branching ratios and detection efficiencies, their contamination to the $\Lambda K^+\pi^-$ channel was found less than 5% at 90% confidence level.

In Fig.17 the momentum distributions of K^+ and π^- are shown for the detected events (upper part) and those corrected for acceptance (bottom part). The behaviour of the acceptance is shown in the middle of Fig.17. These distributions are rather interesting for what concerns the mechanism of Λ production in deuterium. For instance, if Λ is created through rescattering of kaons

$$(pp)n \to K^+(K^-n) \to K^+\pi^-\Lambda \tag{43}$$

then the momentum of K^+ should keep the memory about its value in the primary reaction $pp \to K^+K^-$ and be around 800 MeV/c (smeared by the Fermi-motion of the proton in deuterium).

If Λ's are created from pion rescattering:

$$(pp)n \to \pi^-(\pi^+n) \to \pi^-K^+\Lambda \tag{44}$$

then π^- must have the primary momentum of about 928 MeV/c. These values of "primary" momenta in the binary reaction of $\bar{p}p$ annihilation are shown in Fig.17 by the arrows.

One can see that the observed distributions of kaon and pion momenta do not seem to exhibit the enhancement at the corresponding "primary" momenta.

These distributions are in better agreement with the hypothesis that Λ come from the K^* rescattering:

$$(pp)n \to K^+(K^{*-}n) \to K^+\pi^-\Lambda \tag{45}$$

In this case the K^+ momentum should be around 620 MeV/c and indeed the average momentum of K^+ after correction on acceptance is 680 MeV/c.

The distributions of Λ momentum and of the invariant mass of the $K^+\pi^-$ system are shown in Fig.18.

One should note that Λ events with high momenta dominate. This feature resembles the kinematical properties of the Pontecorvo reaction

$$\begin{aligned} p + d \;&\to\; K^{*0} + \Lambda \\ &\qquad K^{*0} \to K^+ + \pi^- \end{aligned} \tag{46}$$

Then one should see the peak in the invariant mass of K^* and the peak of Λ with a momentum of 1.03 GeV/c. Indeed, there are some events in these regions. However, they do not form any enhancement in, for instance, the invariant mass of $K^+\pi^-$ (see Fig.18). So only the estimation of the upper limit of this reaction can be given. Reaction (46) was

simulated and defined the width of the expected distribution of the invariant mass of $K^+\pi^-$ pairs. There are 11 events at the confidence level of 95% in the region of K^* mass. Then the upper limit for the branching ratio of reaction (46) is equal to $3.5 \cdot 10^{-5}$.

5.3 $\bar{p} + d \to \Lambda + K^+ + \pi^- + \pi^0$

This reaction was selected as the previous one but some differences were present. In this case one has a 1C kinematical fit and a cut on the missing mass for the reaction $\bar{p}d \to \Lambda K^+\pi^- X$ to reduce the contamination from other channels was introduced.

In Fig.16d the invariant mass of the $p\pi^-$ system for the events that passed the selection criteria is shown. In the mass region of Λ a signal is present and it contains 54±8 events. Afeter a fit with a gaussian, the parameters are $M = 1115.9 \pm 0.4$ MeV and $\sigma = 2.9 \pm 0.4$ MeV.

In Fig.19a, c the distributions of K^+ and π^- momentum are shown. The investigated final state could be reached through different two-step rescattering processes and its interpretation is more complicated than for the $\Lambda K^+\pi^-$ channel. One possibility may be the formation of a K^*K pair with subsequent rescattering of the kaon

$$(\bar{p}p)n \to K^{*0}(K^0 n) \to K^+\pi^-\Lambda\pi^0 \quad (47)$$

$$(\bar{p}n)p \to K^{*0}(K^- p) \to K^+\pi^-\Lambda\pi^0 \quad (48)$$

In this case an enhancement in the invariant mass of the $K^+\pi^-$ system should be seen. The distributions of the invariant mass of $K^+\pi^-$ and of the Λ momentum are shown in Fig.19b,d. Indeed, some bump in the K^* region exists. So again, as for the $\Lambda K^+\pi^-$ channel, there are some indications that the $\bar{p}N \to K^*K$ intermediate states are dominant in Λ hyperon formation.

5.4 The branching ratios of Λ production

The determination of the branching ratios for the reactions of Λ production was done in the same manner as was discussed above in Section 3.5. The geometrical acceptance, trigger efficiency and selection cuts were taken into account. The reactions were simulated assuming phase space.

In the case of the $\Lambda K^+\pi^-\pi^0$ channel the main contamination comes from the two channels:

$$\bar{p}d \to \Lambda K^+\pi^- 2\pi^0 \quad (49)$$

$$\bar{p}d \to \Lambda K_L^0\pi^+\pi^- \quad (50)$$

The contamination from reaction (50) was equal to 10% and subtracted from the branching ratio of reaction (42). The contamination of reaction (49) was estimated about 4% of the B.R.($\Lambda K^+\pi^-\pi^0$).

The number of selected events N, Monte Carlo simulated efficiency $\epsilon(MC)$ and the branching ratios obtained are given in Table 6.

As far as the Pontecorvo reaction

$$\begin{aligned} \bar{p} + d &\to K_S^0 + \Lambda \\ & \quad K_S^0 \to \pi^+ + \pi^- \end{aligned}$$

one event was found which could belong to this reaction at 95% confidence level. The corresponding upper limit is also given in Table 6.

6 Summary and conclusions

The results of the study of $\bar{p}d$ annihilation at rest obtained by the OBELIX spectrometer at LEAR (CERN) have been presented. The main aim of this investigation was to study the OZI-rule violation in the reactions of antiproton annihilation.

The branching ratios of the following reactions

$$\bar{p} + d \longrightarrow \pi^- + \phi + p \tag{51}$$

$$\bar{p} + d \longrightarrow \pi^- + \omega + p \tag{52}$$

were measured for two regions of proton momenta: $P < 200$ MeV/c and $P > 400$ MeV/c.

The ratio R=$\phi\pi/\omega\pi$ was found to be

$$\begin{aligned} R\,(\phi\pi^-/\omega\pi^-) = \quad & (133 \pm 26) \cdot 10^{-3} \qquad P < 200 \text{ MeV/c} \\ & (113 \pm 30) \cdot 10^{-3} \qquad P > 400 \text{ MeV/c} \end{aligned}$$

The errors are statistical, the systematic error in the branching ratios determination was estimated to be $\epsilon_{sys} = ^{+5.4}_{-16}$ %.

The values of R are considerably higher than the OZI predictions (2) $R = (0.15\text{–}4.2)\cdot 10^{-3}$.

These results, expressed in terms of the degree of the OZI rule violation (parameter Z from (26)), show that

$$|Z| \geq 0.29 \pm 0.03 \tag{53}$$

The OZI-rule demands that $Z = 0$ and it was verified in different experiments on πp, pp scattering or $\bar{p}p$ annihilation at different energies (for review,see [1],[30]-[34]) that the OZI-rule is broken at most at the order of 6-10%.

The very fact of the strong OZI rule breaking in the antinucleon-nucleon annihilation at rest is firmly established now in different experiments at LEAR [2],[3],[11]. The reasons why just the annihilation at rest is so particular among all other hadronic interactions are not clear. The model of the polarized strange sea in the nucleon [34] attribute this feature of the annihilation at rest to the fact that in the protonium atom the creation of the $\phi\pi$ system comes from the state with 100% polarization of the nucleons (spin triplet $^3S_1$). There are a number of predictions of this model [34] which deserve a dedicated investigation. If this model will be confirmed, it means that the OZI–rule itself is valid but the proton structure is more complicated than that followed from naive constituent quark models. The strangeness components of the nucleon wave function will lead to the ϕ production via connected quark diagrams.

Different exclusive channels of $\bar{p}d$-annihilation were also studied. The excitation of the Δ^{++}-resonance was observed for the first time among the final state products of $\bar{p}d$ annihilation. In agreement with the theoretical predictions of [55] it was possible to see this effect only in the sample with high proton momenta.

The broad enhancement in the 4π invariant mass at $m = 1497 \pm 8$ MeV with the width $FWHM = 177 \pm 14$ MeV was seen in the region of the previously observed [12] $\xi(1480)$ state. It was confirmed the effect seen by the ASTERIX collaboration [13], according to which the position of this peak changes with the increasing of the momentum of proton. The present analysis shows that the shifting of this broad resonance is due to the shrinkage of the available phase space for events with high proton momenta.

The positions of ω, ρ and $f_2(1270)$ were not observed to change with the proton momentum.

The measurements of the branching ratios of different channels of $\bar{p}d$ annihilation show that the branching ratios decrease with proton momenta practically by the same factor.

Some indications that the $pN \to K^*K$ intermediate states are dominant in Λ hyperon formation were obtained.

7 Acknowledgments

We would like to thank the technical staff of the LEAR machine group for their support during the runs.

We are very grateful to D.Buzatu, F.M.Lev, M.P.Locher and B.S.Zou for providing us with the results of their calculations before publications. We thanks V.M.Kolybasov for interesting discussions.

The JINR group acknowledges the support from the Russian Fund of Fundamental Research under grant No.93-02-3997 as well as from the International Science Foundation, grant No. ML9000.

Table 1. Branching ratios of the ϕ and ω-meson production for different regions of the proton momentum P.

Final state P (MeV/c)	$\phi + \pi^- + p_s$ <200	$\phi + \pi^- + p$ 400-1000	$\omega + \pi^- + p_s$ <200	$\omega + \pi^- + p$ 400-1000
N. events	859 ± 57	38 ± 6	222 ± 39	499 ± 63
$\epsilon(MC) \cdot 10^3$	10.0 ± 0.2	3.00 ± 0.09	95 ± 5	2.40 ± 0.06
B.R.$(pd) \cdot 10^4$	6.62 ± 0.49	0.95 ± 0.22	49.7 ± 8.9	8.38 ± 1.09
B.R.$(\bar{p}n) \cdot 10^4$	14.8 ± 1.1		111 ± 20	

Table 2: Branching ratios of $\bar{p}n$ and $\bar{p}p$ annihilation with proton and neutron-spectators

Final state	N. events	$\epsilon(MC)$,%	B.R., % OBELIX	Other experiments	Refs.
$2\pi^-\pi^+$	745	11.6 ± 0.1	2.71 ± 0.11	1.57 ± 0.21	[10]
				3.4 ± 0.2	[39]
				2.4 ± 0.4	[9]
$2\pi^-2\pi^+$	2024	12.8 ± 0.1	5.40 ± 0.20	6.9 ± 0.6	[42]
$3\pi^-2\pi^+$	1079	7.7 ± 0.2	5.90 ± 0.22	5.15 ± 0.47	[10]
				6.9 ± 0.5	[41]
				4.2 ± 0.2	[39]
$3\pi^-3\pi^+$	252	3.43 ± 0.29	2.51 ± 0.21	2.1 ± 0.2	[42]

Table 3. Fitted values of the resonance positions for two regions of the proton momenta.

Resonance	$P < 200\ MeV/c$	$P = 400 - 800\ MeV/c$
ω	772 ± 5	782.0 ± 3.1
ρ	739 ± 15	734 ± 9
$f_2(1270)$	1291 ± 8	1252 ± 10
$\xi(1480)$	1497 ± 8	1318 ± 12

Table 4: Branching ratios of $3\pi p$ and $\pi^-\omega p$ final states at different momenta of the proton.

Proton Momentum, GeV/c	B.R. $(\omega\pi^- p) * 10^4$	B.R.$(2\pi^-\pi^+ p) * 10^4$
0.4-0.5	1.41 ± 0.20	4.46 ± 0.32
0.5-0.6	1.33 ± 0.36	4.07 ± 0.36
0.6-0.7	1.49 ± 0.51	4.04 ± 0.49
0.7-0.8	1.80 ± 0.73	4.02 ± 0.60

Table 5. Branching ratios (in 10^{-4}) of annihilation channels in two regions of proton momenta. The ratio of B.R.(400-800)/B.R.(<200) is shown in the last column.

Final state	B.R.$(P < 200\ MeV/c)$	B.R.$(P = 400 - 800\ MeV/c)$	Ratio
$2\pi^-\pi^+$	150 ± 6	16.6 ± 0.9	9.0 ± 0.6
$3\pi^-2\pi^+$	326 ± 12	44 ± 7	7.4 ± 1.2
$\pi^-\phi$	6.62 ± 0.49	0.95 ± 0.22	7.0 ± 1.7
$\pi^-\omega$	49.7 ± 8.9	8.38 ± 1.09	5.9 ± 1.3

Table 6. Branching ratios for Λ production in $\bar{p}d$ annihilation (in 10^{-4}).

Final state	N events	$\epsilon(MC) * 10^3$	B.R.(OBELIX)	B.R.([56])
$\Lambda K^+\pi^-$	35 ± 7	2.1 ± 0.1	0.96 ± 0.19	0.3 ± 0.2
$\Lambda K^+\pi^-\pi^0$	54 ± 8	0.57 ± 0.05	3.5 ± 0.8	2.1 ± 0.4
ΛK^{*0}	11*)		< 0.35, 95%$C.L.$	
ΛK^0	1**)		< 0.63, 95%$C.L.$	

*) 11 events of the $\Lambda K^+\pi^-$ final state with the $K^+\pi^-$ invariant mass in the region of K^* were seen, however they do not form any peak, so these events were used for an estimation of the upper limit for the Pontecorvo reaction $\bar{p}d \to \Lambda K^* \to \Lambda K^+\pi^-$.

**) one event passing through the cuts on the Pontecorvo reaction $\bar{p}d \to \Lambda K^0$ could be used only for the estimation of the upper limit.

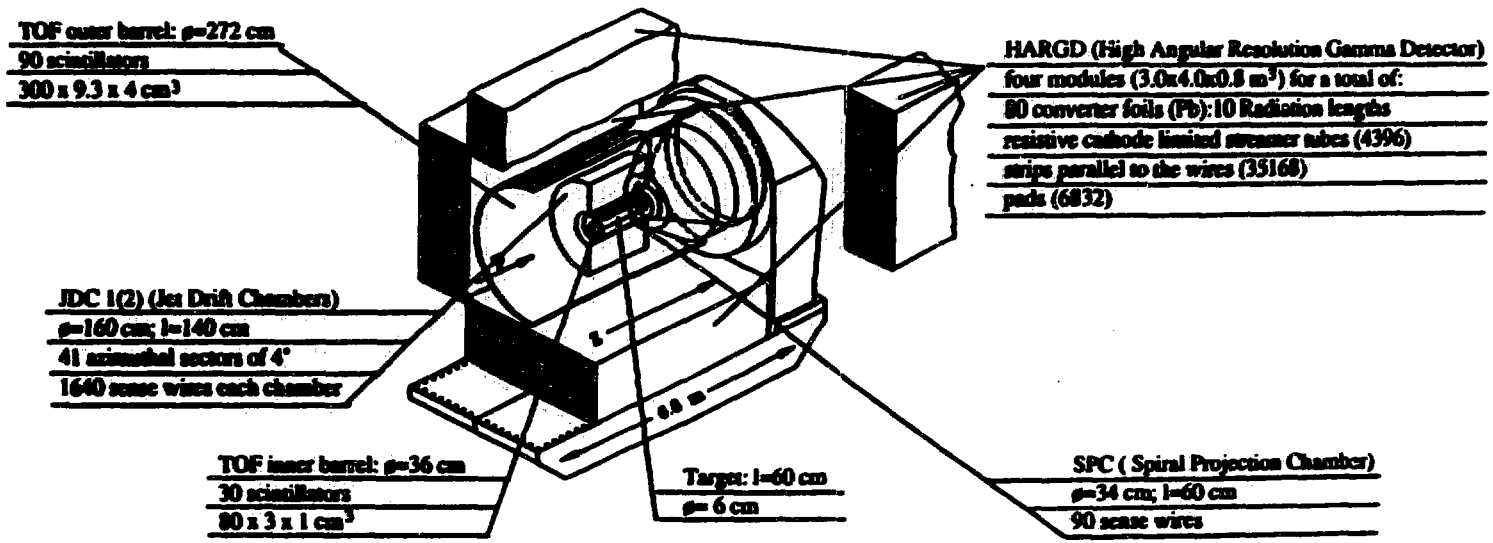

Figure 1: Layout of the OBELIX spectrometer.

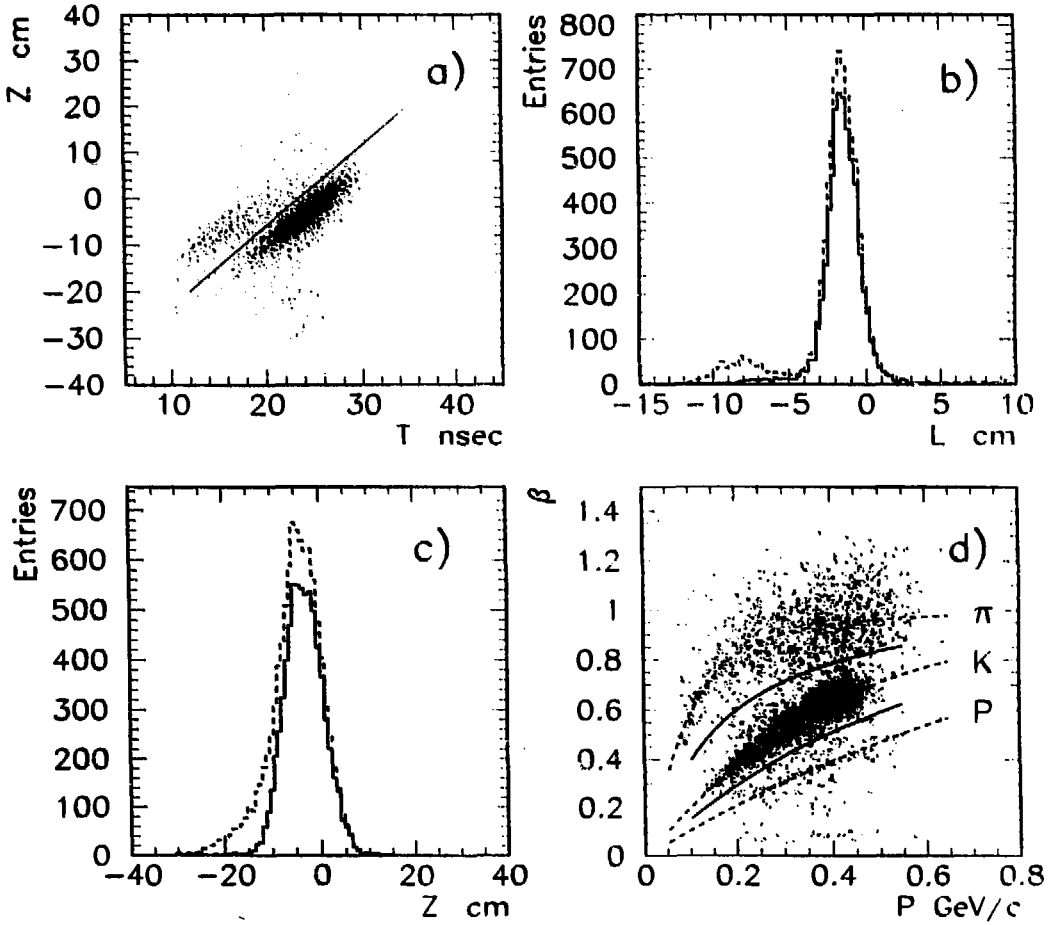

Figure 2: a) The distribution of the minimum times in the inner TOF slabs for the annihilation events with different z-coordinates of the vertex. The z=0 point corresponds to the middle of the target. Mylar and target annihilations can be separated by a straight line.
b) The distribution of the annihilation times projected on the line shown in Fig.2a (dashed line). The solid line corresponds to the distribution of the annihilation times occurring within the 16 ns gate signal, delayed by 20 ns from the antiproton arrival.
c) The distribution of the annihilation vertices along the beam axis. The dashed line corresponds to the distribution without demand on the time gate, the solid line is the z-distribution of the vertices within the time gate. The target entrance and exit windows are at ∓ 31 cm.
d) The distribution of velocity β for the particles with different momenta. Solid lines correspond to the corridor used for the kaon selection.

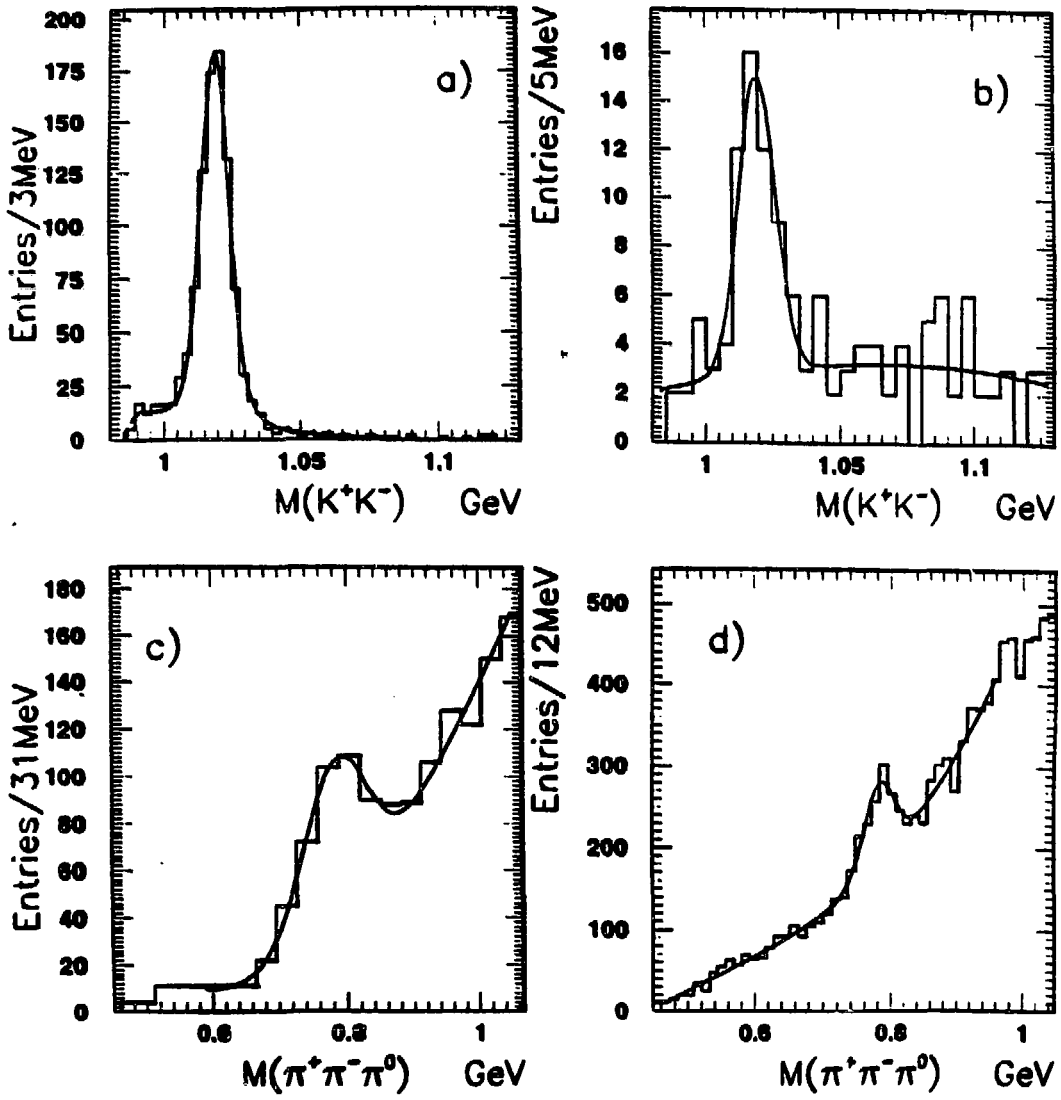

Figure 3: Invariant mass distribution of the K^+K^- system in the reaction $p + d \rightarrow \pi^- + K^+ + K^- + p$ for the proton-spectator region (P<200 MeV/c) (a) and for proton momenta P>400 MeV/c (b). Invariant mass distribution of the $\pi^+\pi^-\pi^0$ system for the reaction $p+d \rightarrow 2\pi^- + \pi^+ + \pi^0 + p$ for the proton-spectator region (c) and for high proton momenta (d).

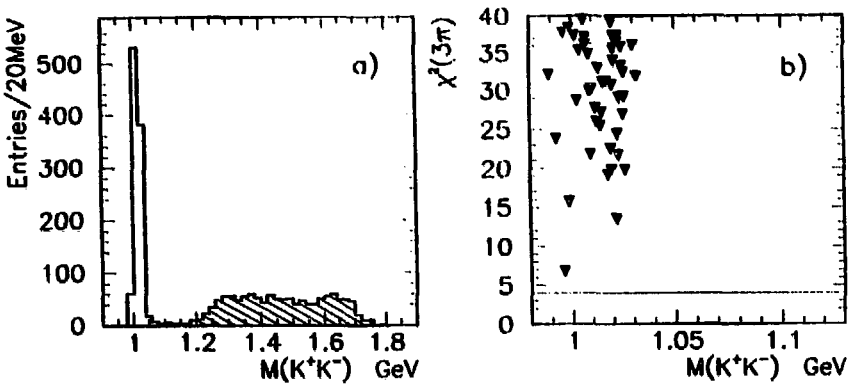

Figure 4: a) The invariant mass distributions of different pairs of particles that passed all selection criteria. The open histogram corresponds to the sum of all three possible combinations of two kaons: (13),(23) and (12), the hatched part of the histogram corresponding to the "wrong" combinations (13) and (12).
b)Test of the contamination from the reaction $\bar{p} + d \rightarrow 3\pi p_s$ for events that passed the selection criteria for $\bar{p} + d \rightarrow K^- K^+ \pi^- p_s$ channel. The χ^2 for the 3π hypothesis versus the K^+K^- invariant mass is plotted. The line indicates the 5% CL

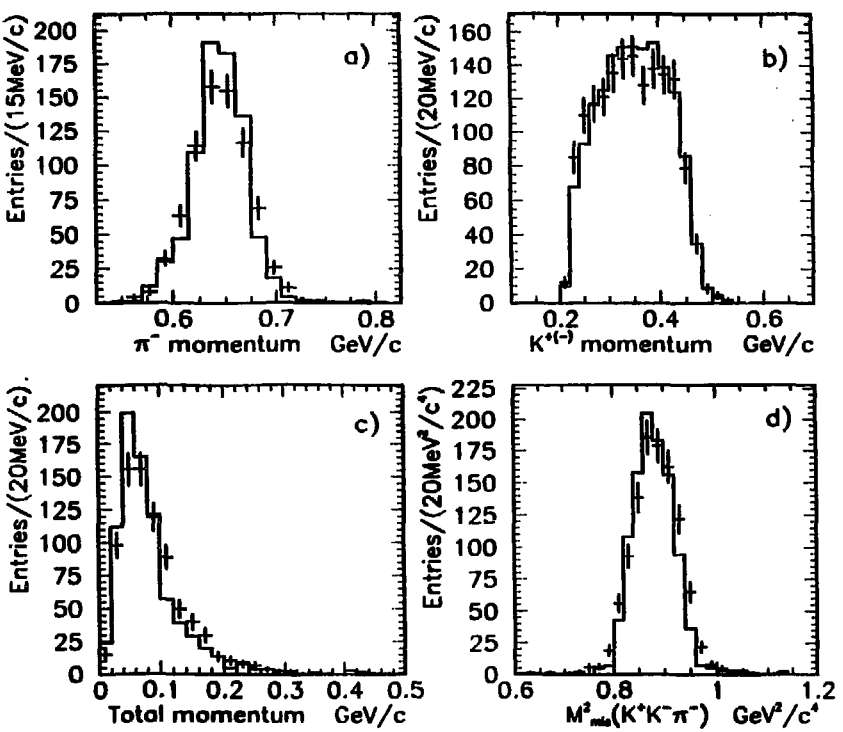

Figure 5: Comparison between the results of the Monte Carlo simulations (crosses) and the experimental data (solid line). (a) Momentum distribution of negative pions; (b) momentum distribution of kaons; (c) the distribution of the total momentum of particles in JDC $\mathbf{P_{tot}} = \mathbf{p_1} + \mathbf{p_2} + \mathbf{p_3}$, (d) missing mass squared distribution.

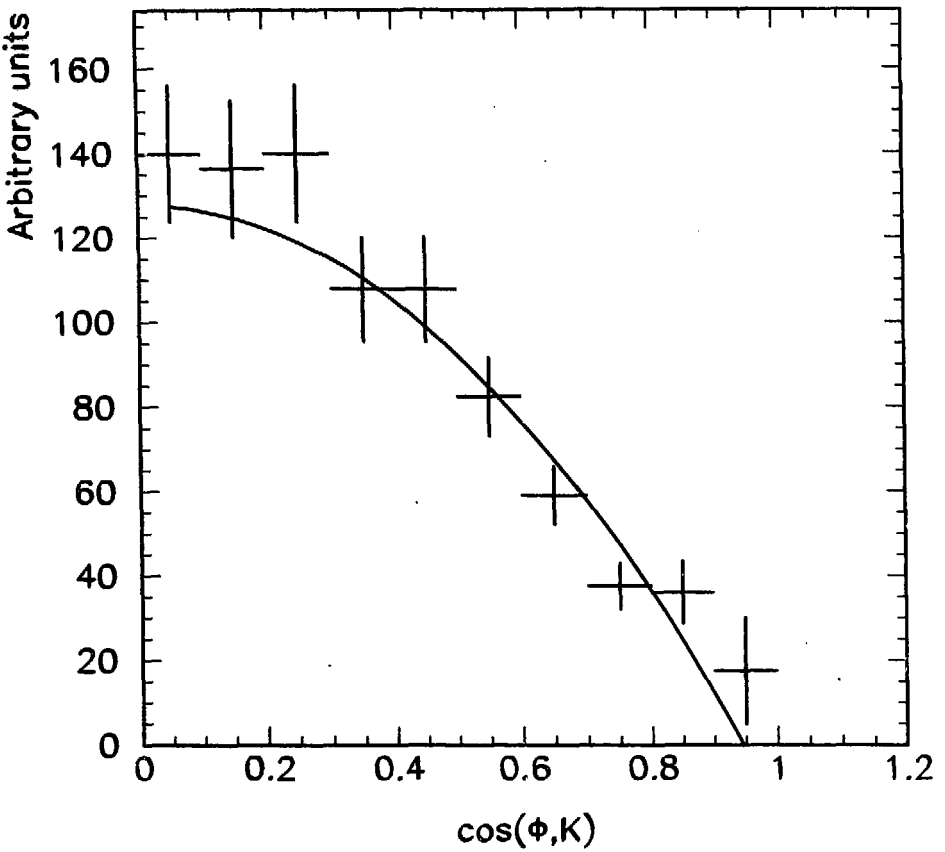

Figure 6: The $\phi \to K^+K^-$ decay angular distribution in the reaction $\bar{p} + d \to \pi^- + \phi + p_s$. θ is the angle between the fast kaon with respect to the ϕ momentum in the K^+K^- rest frame. The solid line corresponds to the $\sin^2\theta$ dependence expected for annihilation from the $^3S_1$ state.

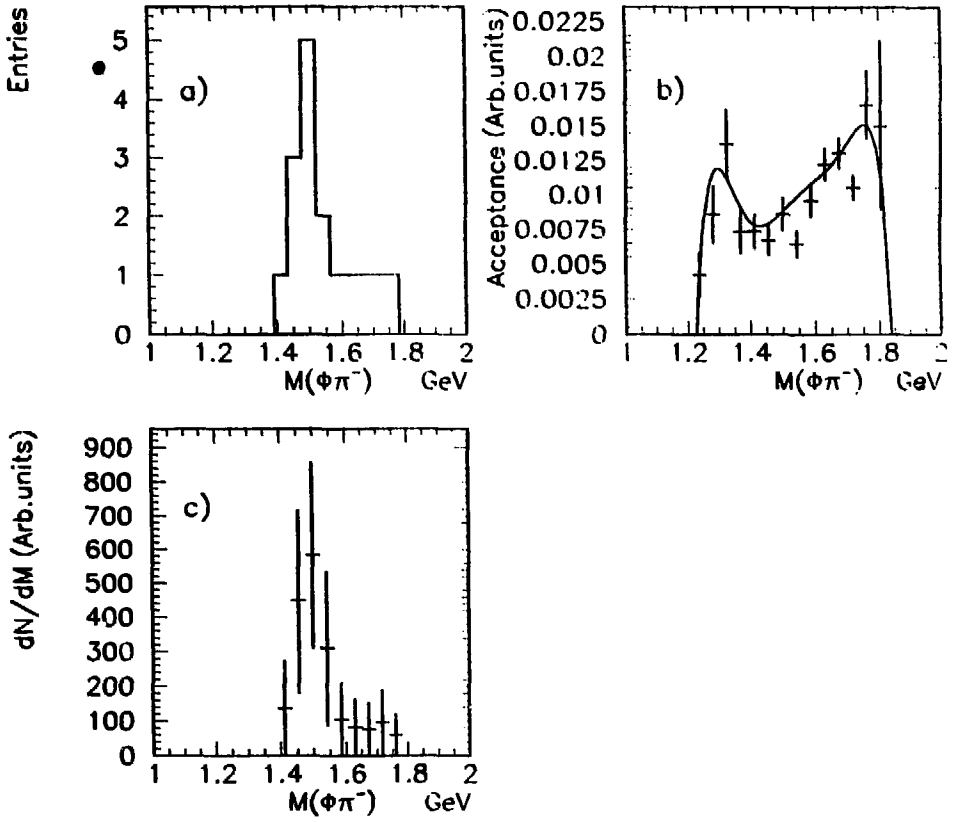

Figure 7: The invariant mass distribution of the $\phi\pi^-$ system at high proton momenta ($P > 400\ MeV/c$). a) experimental distribution not corrected for the acceptance; b)acceptance of the apparatus simulated by the Monte Carlo; c)experimental distribution corrected for the acceptance.

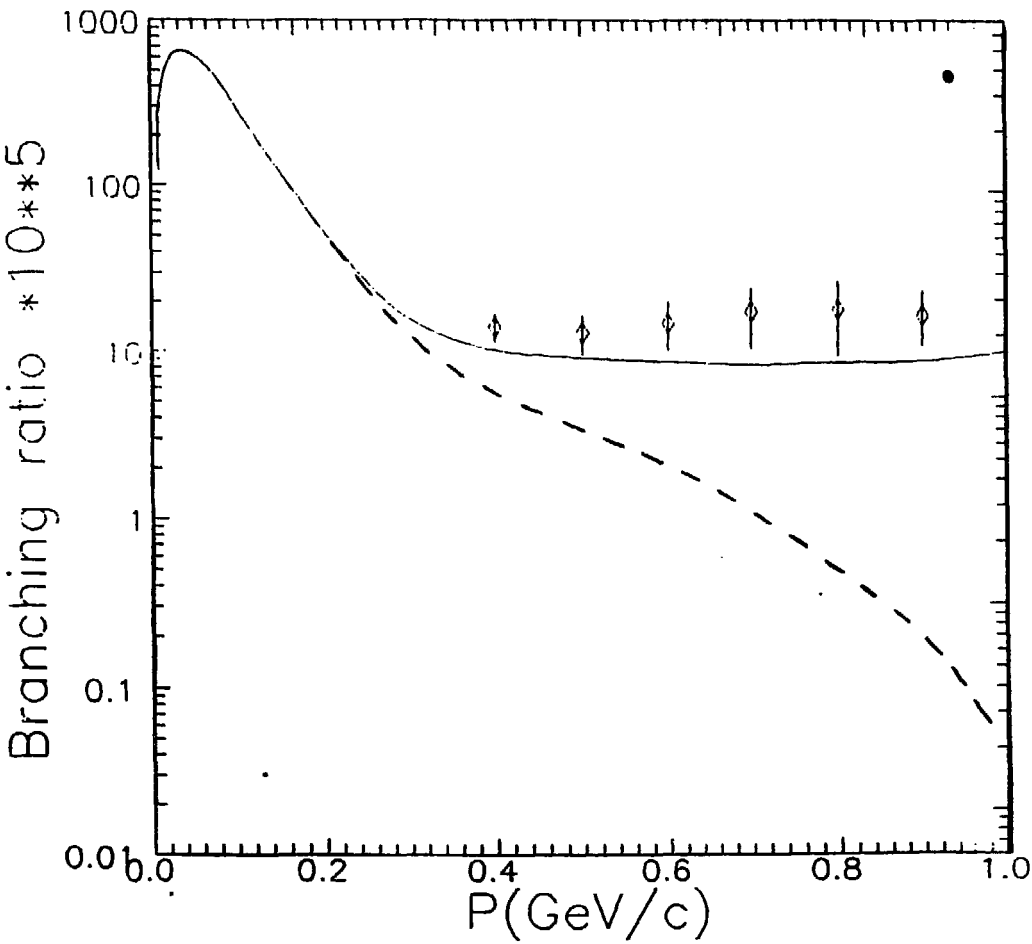

Figure 8: The yield of ω for different proton momenta. The solid line corresponds to the result of the calculations of F.Lev and D.Buzatu [27] normalized to the experimental yield of $\omega\pi$ in the proton-spectator region. The dashed line corresponds to the calculations where rescattering of annihilation mesons was not taken into account.

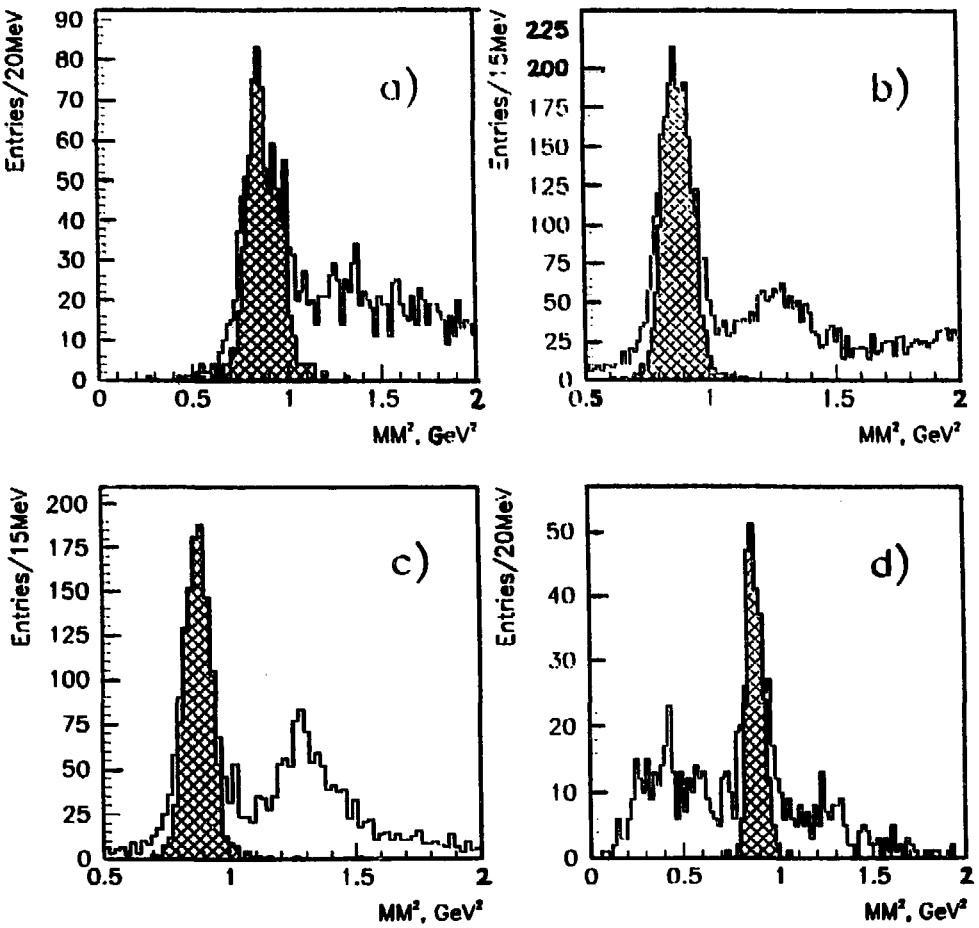

Figure 9: The distributions of the missing mass squared MM^2 for the reactions with 3 (a),4 (b), 5 (c) and 6 (d) charged pions in the final state. $MM^2 = (M_p + M_d - \sum_i E_i)^2 - P_{tot}^2$, where E_i are the energies of charged pions and P_{tot} is the total momentum of charged pions. The solid lines correspond to the distributions when the nucleon-spectator cut of $P_{tot} < 200\ MeV/c$ was applied. The hatched histograms correspond to the events which have the confidence level for the investigated hypothesis greater than 10%.

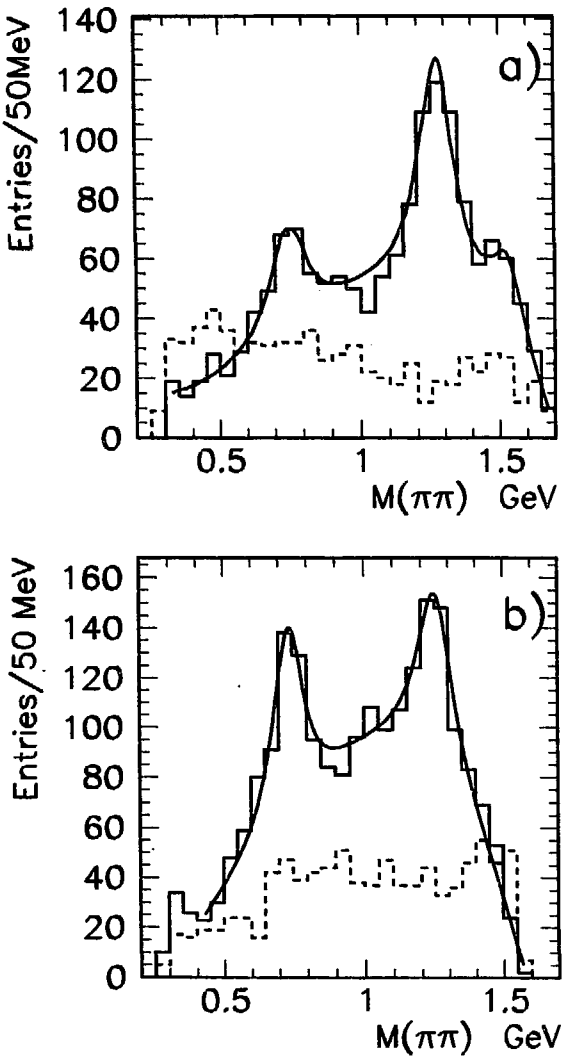

Figure 10: The invariant mass distribution of the $\pi^+\pi^-$ (solid line) and $\pi^-\pi^-$ (dashed line) systems in the reaction $\bar{p}d \to 2\pi^-\pi^+p$ for the proton-spectators ($P < 200$ MeV/c) (a) and for annihilation with high-momenta protons ($P > 400$ MeV/c) (b).

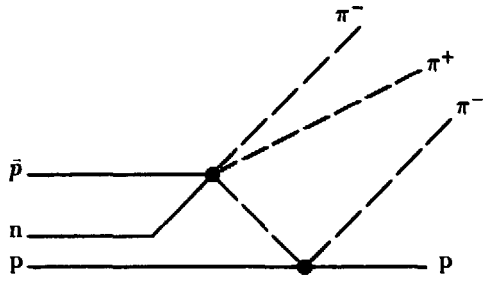

a)

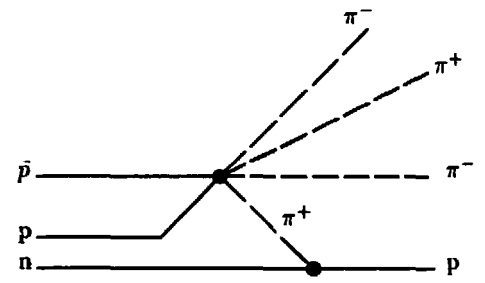

b)

Figure 11: Diagrams of the meson rescattering (a) and the Pontecorvo reaction (b) for the reaction $pd \to 2\pi^-\pi^+p$

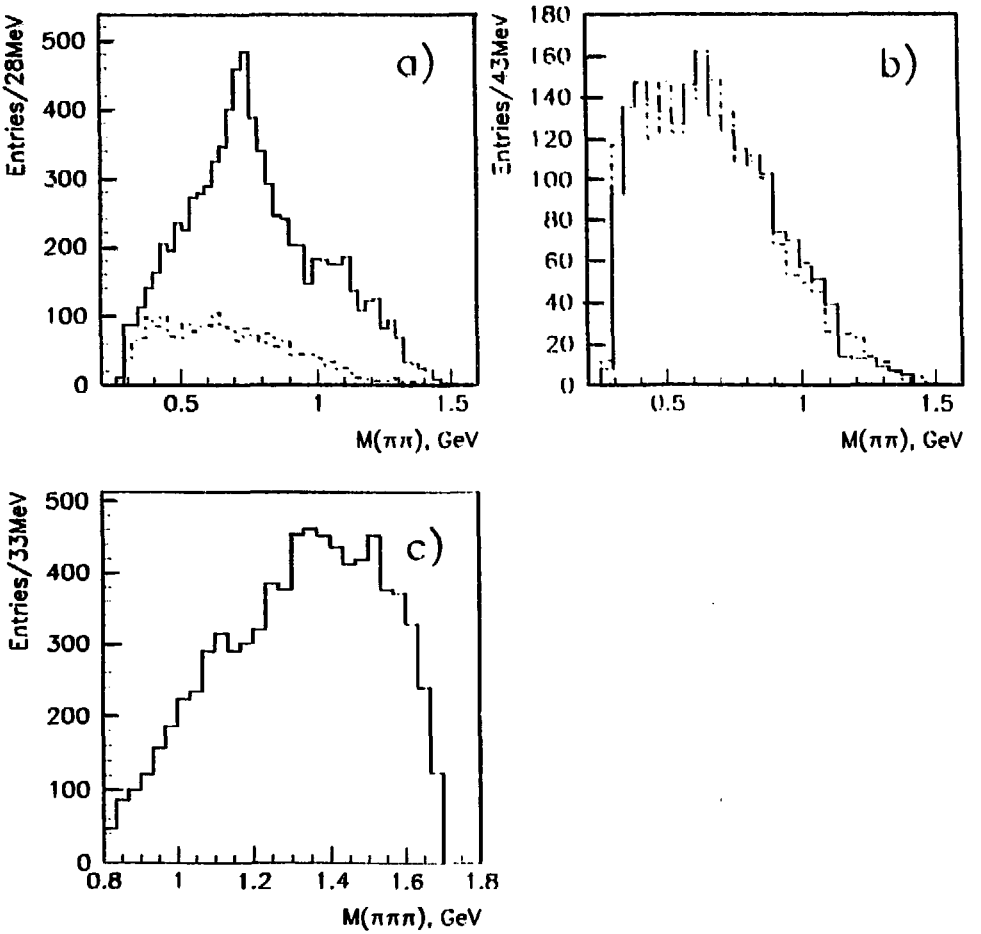

Figure 12: Invariant mass distributions of different pion systems in the reaction $\bar{p}d \rightarrow 2\pi^-2\pi^+n$:
(a) $\pi^+\pi^-$ (solid line) and $\pi^-\pi^-$ (dashed line);
(b) $\pi^-\pi^-$ (solid line) and $\pi^+\pi^+$ (dashed line);
(c) $\pi^+\pi^-\pi^\pm$

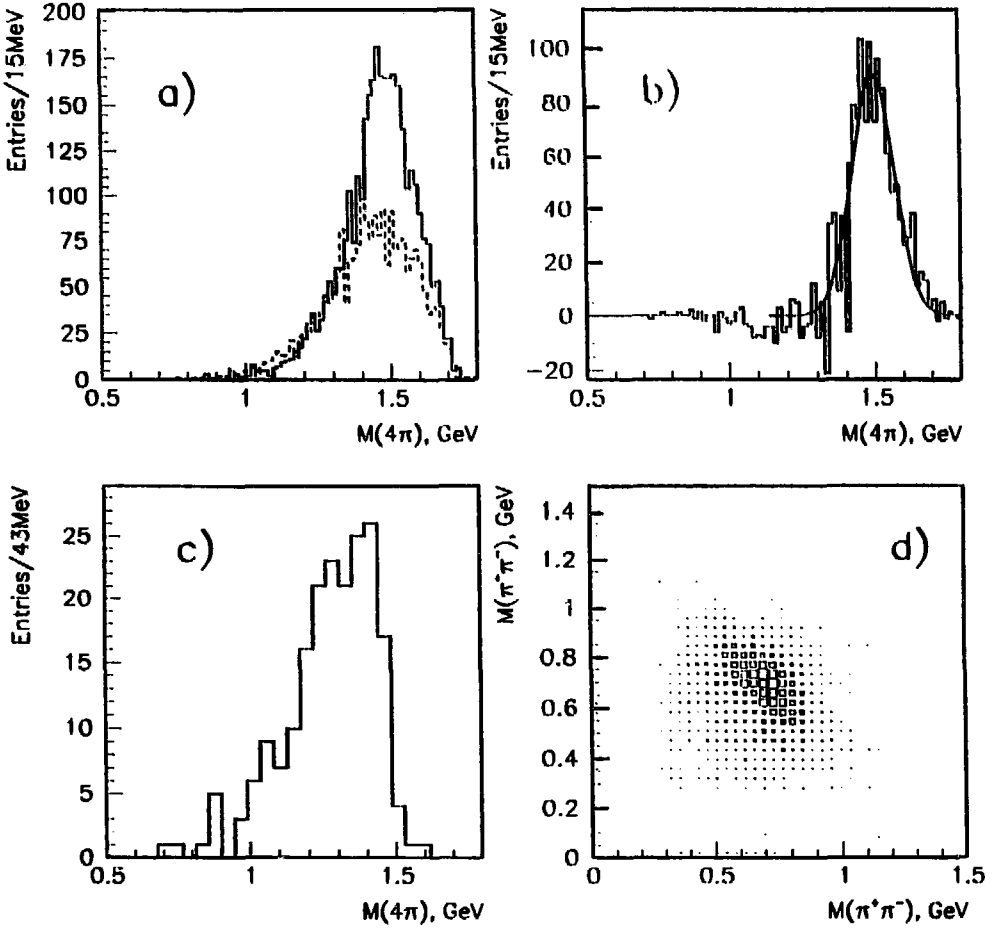

Figure 13: The invariant masses of the 4π system in the reaction $\bar{p}d \rightarrow 3\pi^- 2\pi^+ p$.
(a) The solid line corresponds to the invariant mass of the $2\pi^+ 2\pi^-$ system and the dashed line is for the $\pi^+ 3\pi^-$ one.
(b) The difference spectrum obtained after subtraction of the background $3\pi^- \pi^+$ from the $2\pi + 2\pi^-$ distribution.
(c) The invariant mass of 4π for events with high proton momenta (p>400 MeV/c).
(d) The scatter plot of the invariant masses of dipions $\pi^+\pi^-$ (for events with p<200 MeV/c).

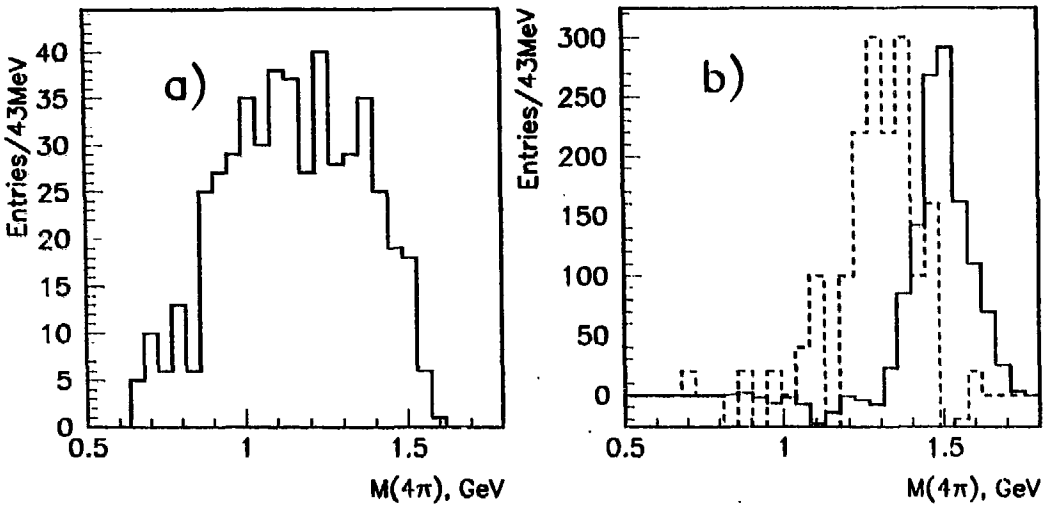

Figure 14: (a) The Monte Carlo simulation of the invariant mass distribution of the 4π system in the reaction $\bar{p}d \rightarrow \pi^- X(1480)p$ assuming flat proton momentum spectrum for P>400 MeV/c. b)The difference spectrum of the 4π system for the sample with $P_{tot} < 200$ MeV/c (solid line) and for the data with $P_{tot} > 400$ MeV/c (dashed line). The latter histogram is multiplied by 20.

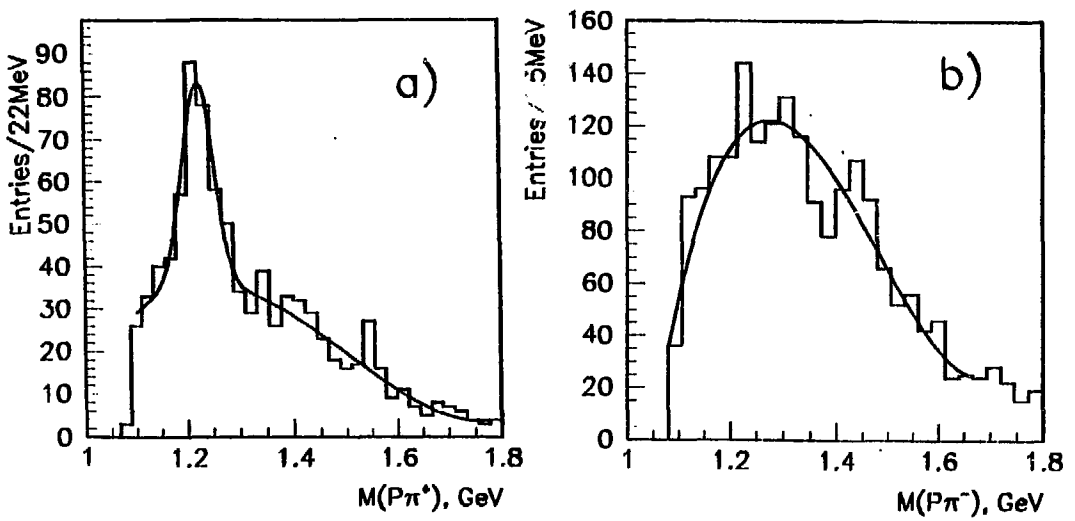

Figure 15: The invariant mass distributions of the $\pi^+ p$ (a) and $\pi^- p$ systems (b) in the reaction $\bar{p} + d \rightarrow \pi^+ + 2\pi^- + p + m\pi^0, \quad m = 0, 1, 2...$ for the protons with momenta P> 400 MeV/c.

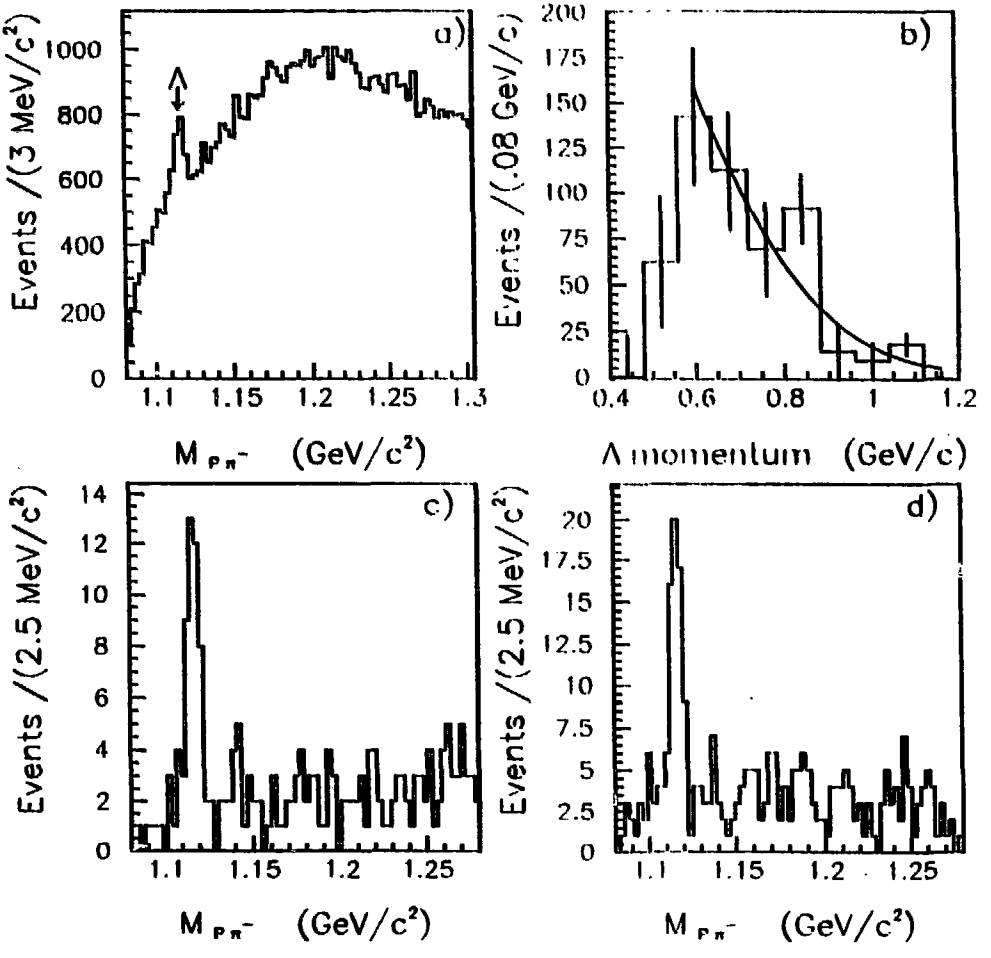

Figure 16: a) The invariant mass of $p\pi^-$ pairs.
b) The Λ momentum distribution (not corrected for the acceptance).
c) The invariant mass of $p\pi^-$ pairs in the reaction $pd \rightarrow \Lambda K^+\pi^-$.
d) The invariant mass of $p\pi^-$ pairs in the reaction $pd \rightarrow \Lambda K^+\pi^-\pi^0$.

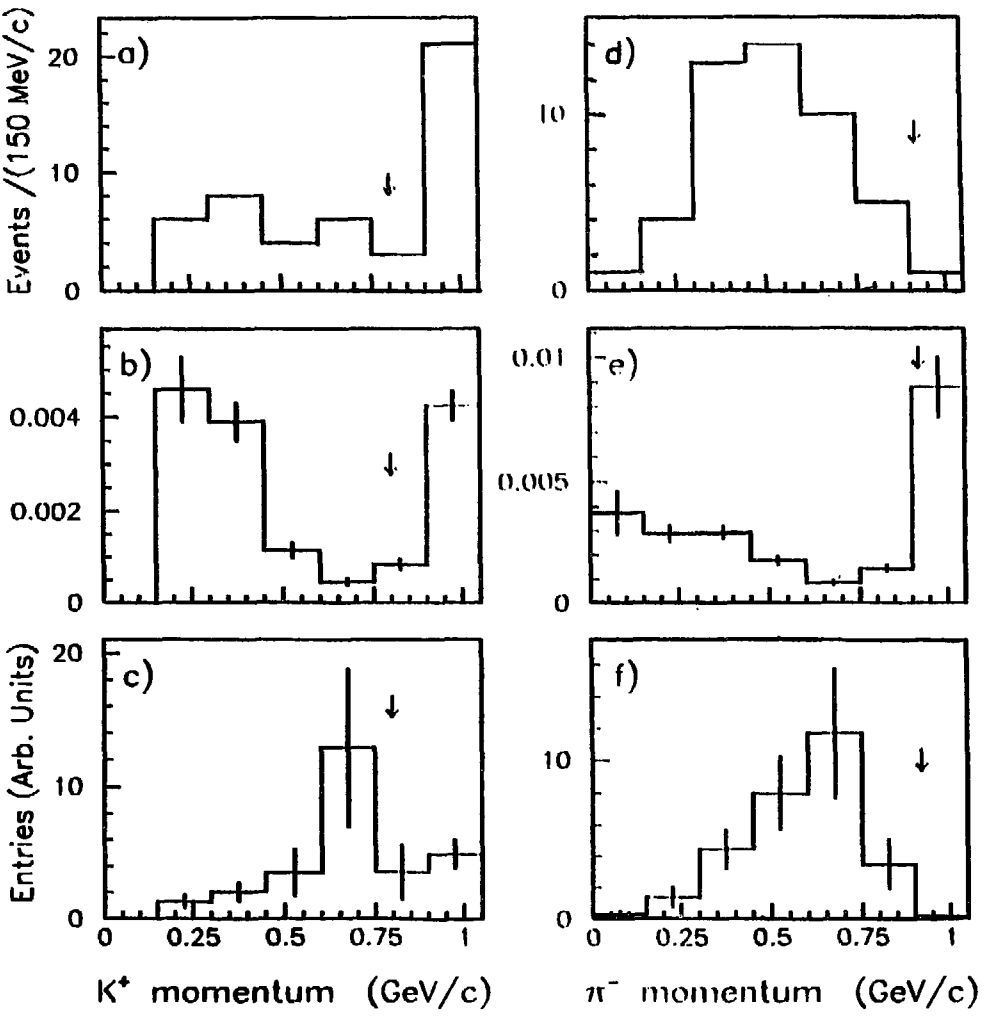

Figure 17: a),d) The distributions of K^+ and π^- momenta for the events under the peak of Λ in reaction (41), respectively. b),e) The distributions of the acceptances of these values in reaction (41). c),f) The distributions of K^+ and π^- momentum, corrected for the acceptances.

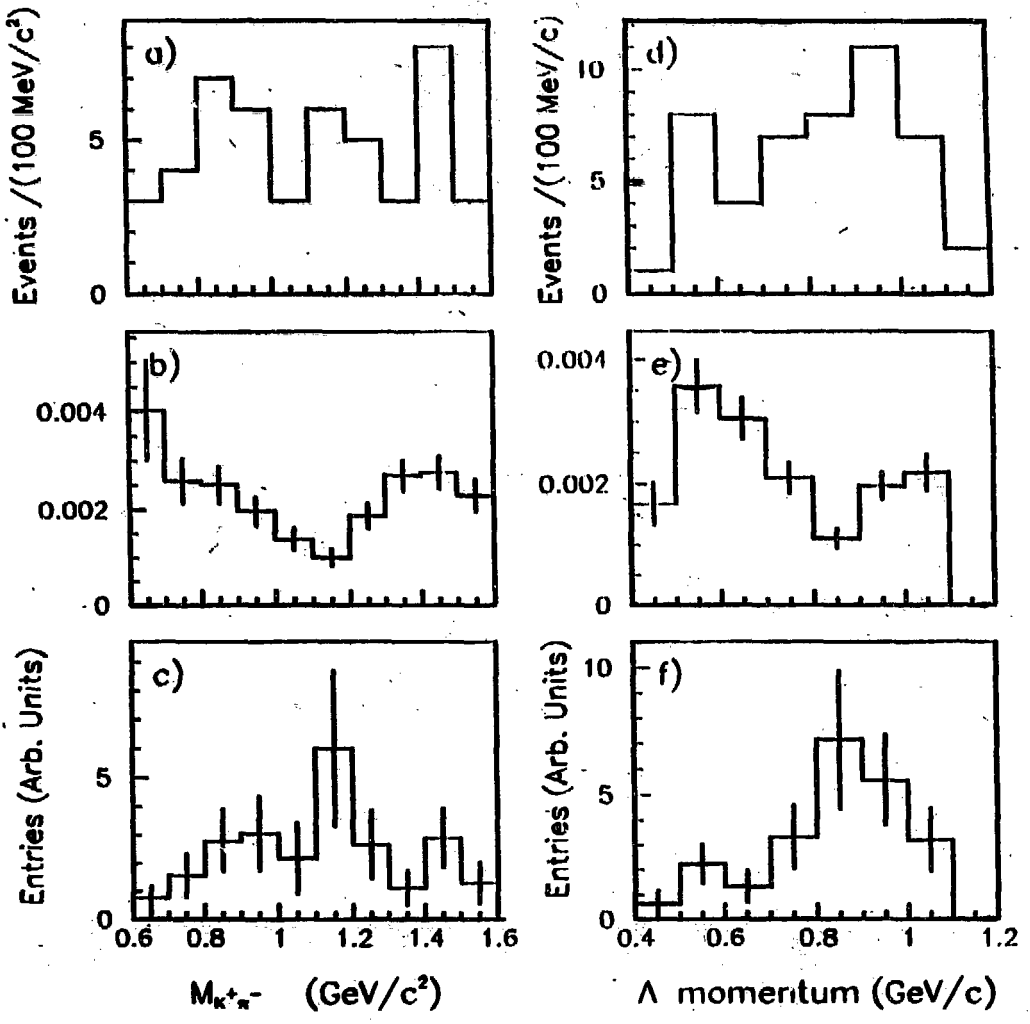

Figure 18: a) The distribution of the invariant mass of the $K^+\pi^-$ system for the detected events under the peak of Λ in reaction (41). b) The distribution of the acceptance of this value in reaction (41). c) The reconstructed distribution of the invariant mass of the $K^+\pi^-$ system. d) The total momentum distribution of $p\pi^-$ pairs for the detected events in reaction (41). e) The distribution of the acceptance of this value in reaction (41). f) The reconstructed distribution of the total momentum of $p\pi^-$ pairs.

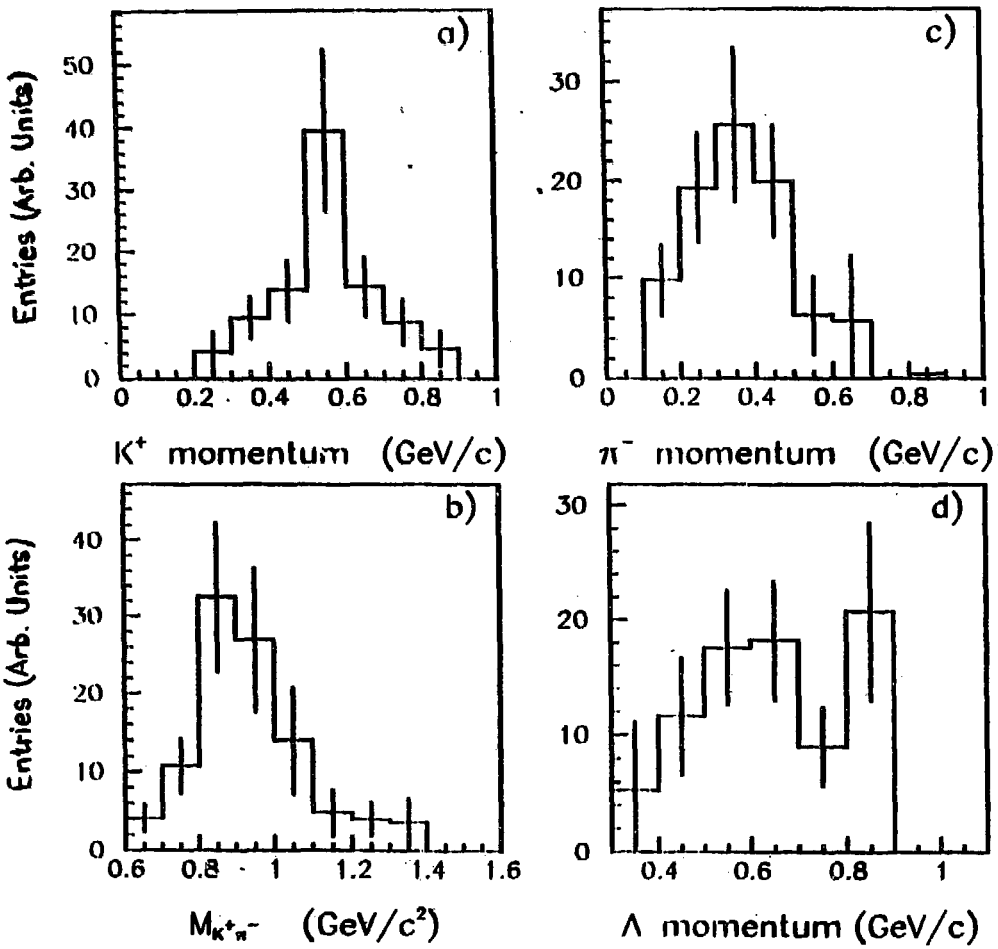

Figure 19: a),c),d) The distributions of K^+, π^- and Λ momenta in reaction (42), respectively. b) The distribution of the invariant mass of the $K^+\pi^-$ system in reaction (42).

References

[1] A.M. Cooper et al., Nucl.Phys., B146 (1978) 1.

[2] J.Reifenrother et al., Phys.Lett., B267 (1991) 299.

[3] M.A.Faessler et al., Proc. NAN-93 Conference, Moscow, 1993.

[4] S.Okubo, Phys.Lett. 5 (1963) 165; G. Zweig, CERN Report TH 412 (1964); I.Iizuka. Prog. Theor. Phys. Suppl. 37-38 (1966) 21.

[5] H.J.Lipkin , Phys.Lett., B60 (1976) 371.

[6] Review of Particle Properties, Phys.Rev. D45 (1992) Part II.

[7] R.Bizzarri R. et al., Nuov.Cim., 20A (1974) 393.

[8] A.Bettini et al., Nuov.Cim., 63A (1969) 1199.

[9] R.Bizzarri et al., Phys.Rev.Lett, 25 (1970) 1385.

[10] A.Bettini et al., Nuov.Cim., 47A (1967) 642.

[11] V.G.Ableev et. al., Proc. Hadron-93 Conference, Como, 1993 and Phys. Lett. B, in press.

[12] L.Gray et al., Phys.Rev., D27 (1983) 307.

[13] P.Weidenauer et al., Z.Phys., C59 (1993) 387.

[14] F.Balestra et al., Nucl.Phys., A526 (1991) 415.

[15] J.Cugnon , J.Vandermeulen , Phys.Rev., C39 (1989) 181.

[16] D.E.Kharzeev, M.G.Sapozhnikov , Nuov.Cim., 104A (1991) 1509.

[17] A.M.Rozhdestvensky, M.G.Sapozhnikov, Surveys in High Energy Physics, 6 (1992) 115.

[18] A.Adamo et al., Sov.J.Nucl.Phys., 55 (1992) 1732.

[19] M.P.Locher, A.Svarc, Z.Phys. A338 (1991) 89.

[20] A.Adamo et al., Phys.Lett., B284 (1992) 448.

[21] M.P.Locher, B.S.Zou, Few-Body Systems, 12 (1992) 1.

[22] Zou B.S., private communication.

[23] D.E.Kharzeev et al., Sov.J.Nucl.Phys., 55 (1992) 1212; JINR preprint E91-104, 1991, Dubna.

[24] S.I.Bityukov et al., Phys.Lett., B188 (1987) 383.

[25] F.Close, H.Lipkin, Phys.Lett., B196 (1987) 245.

[26] C.Dover, P.Fishbane, Phys.Rev.Lett. 62 (1989) 2917.

[27] F.M.Lev and D.Buzatu, submitted to Yad.Fiz.

[28] R.Bizzarri et al., Nuov.Cim., 22A (1974) 225.

[29] C.Amsler et al., Z.Phys., C58 (1993) 175.

[30] S.Okubo, Phys.Rev., D16 (1977) 2336.

[31] C.B.Dover et. al., Prog.Part.Nucl.Phys., 29 (1992) 87.

[32] J.Ellis, E.Gabathuler, M.Karliner, Phys.Lett., B217 (1989) 173.

[33] J.Ellis , M.Karliner, Phys.Lett. B313 (1993) 407.

[34] J.Ellis et al., CERN preprint, TH/94-7326, Geneva, 1994.

[35] K.Braune et al., Proc.LEAP-92 Conf., Courmayeur, 1992. Nucl.Phys., A558 (1993) 269c.

[36] Y.Lu, B.S.Zou, M.P.Locher, Z.Phys., A347 (1994) 281.

[37] D.Buzatu, F.Lev , Phys.Lett.,B329 (1994) 143.

[38] K.Königsmann, CERN preprint, PPE/93-182, Geneva, 1993.

[39] D.Bridges et al., Phys.Rev.Lett., 56 (1986) 215.

[40] A.Bettini et al., Nuov.Cim , 42A (1966) 695.

[41] M.Gaspero , Nucl.Phys., A562 (1993) 407.

[42] R.Armenteros et al., CERN/PSCC/86-4. Updated data of published by R.Armenteros, B.French , High Energy Physics, 4 (1969) 237.

[43] B.May et al., Phys.Lett., B225 (1989) 450.

[44] E.Aker et al., Phys.Lett., B260 (1991) 249.

[45] A.Adamo et al., Phys.Lett., B287 (1992) 368.

[46] A.Zenoni, Proc. NAN-93 Conference, Moscow, 1993.

[47] V.Anisovich et al., Phys.Lett., B323 (1994) 233.

[48] J.Diaz et al., Nucl.Phys., B16 (1970) 239.

[49] D.Bridges et al., Phys.Rev.Lett., 56 (1986) 211; ibid., v.57, p.1534.

[50] A.Lanaro et al, Proc. LEAP-92 Conf., Courmayeur, 1992, Nucl.Phys., A558 (1993) 13c.

[51] A.Feliciello et al., Proc. HADRON-93 Conference, Como, 1993.

[52] C.Amsler et al., Phys.Lett., B322 (1994) 431.

[53] V.M.Kolybasov, I.S.Shapiro, Yu.N.Sokolskikh, Phys.Lett., B222 (1989) 135.

[54] T.E.Kalogeropoulos et al., Phys.Rev., D24 (1981) 1759.

[55] D.V.Voronov, V.M.Kolybasov, JETP Letters, 57 (1993) 162.

[56] R.Bizzari et al.,Lett. Nuovo Cimento 2 (1969) 431.

[57] J.Riedlberger et al.,Phys. Rev. C40 (1989) 2717.

[58] M.Locher, International Conference on Medium- and High-Energy Physics, Taipei, 1988,edited by W.P.Hwang,K.Liu,Y.Tzeng (Syngapore,1989),p.656.

Received by Publishing Department on August 22, 1994.